Electromagnetic analysis and simulation aspects of wireless power transfer in the domain of inductive power transmission technology

Lionel Pichon

Journal of Electromagnetic Waves and Applications

ISSN: (Print) (Online) Journal homepage: https://www.tandfonline.com/loi/tewa20

Electromagnetic analysis and simulation aspects of wireless power transfer in the domain of inductive power transmission technology

Lionel Pichon

To cite this article: Lionel Pichon (2020) Electromagnetic analysis and simulation aspects of wireless power transfer in the domain of inductive power transmission technology, Journal of Electromagnetic Waves and Applications, 34:13, 1719-1755, DOI: 10.1080/09205071.2020.1799870

To link to this article: https://doi.org/10.1080/09205071.2020.1799870

Published online: 30 Jul 2020.

JOURNAL OF ELECTROMAGNETIC WAVES AND APPLICATIONS
2020, VOL. 34, NO. 13, 1719–1755
https://doi.org/10.1080/09205071.2020.1799870

Taylor & Francis
Taylor & Francis Group

INVITED REVIEW PAPER

OPEN ACCESS Check for updates

Electromagnetic analysis and simulation aspects of wireless power transfer in the domain of inductive power transmission technology

Lionel Pichon[a,b]

[a]Group of Electrical and Electronic Engineering of Paris, Université Paris-Saclay, CentraleSupélec, CNRS, Paris, France; [b]Group of Electrical and Electronic Engineering of Paris, Sorbonne Université, CNRS, Paris, France

ABSTRACT

Wireless power transfer (WPT) technologies have now reached a commercial stage in applications going from consumer electronics, biomedical implants and domestic applications. For electrical cars, WPT offers some new opportunities compared to classical wired charging. Although there exist some commercial cars equipped with wireless charging system, improving design procedures needs to address various domains including power electronics, components and electromagnetics. The magnetic coupling system is a key component of wireless power transfer: the coils and surrounding materials have a great impact on the efficiency of the transfer as well as the level of the stray field near the system. The paper aims to present three essential features regarding the inductive power transfer dedicated to electric vehicles. The first one addresses the topology and efficiency of the coupling system, the second one underlines the human exposure considerations and the third one deals with the impact of uncertainties regarding system parameters.

ARTICLE HISTORY
Received 11 February 2020
Accepted 17 July 2020

KEYWORDS
Electromagnetic modeling; wireless power transfer; electromagnetic compatibility; electric vehicle

1. Introduction

In the last decades, the scientific community has studied different mechanisms of the transfer of energy to distances by wireless power transfer (WPT).

Today, this definition covers several technologies in a widespread range of applications, powers and distances [1]. Wireless power transfer technologies based on electromagnetic fields can be divided into two categories according to the coupling region between transmitting antenna and receiving antenna: (1) non-radiative region or near-field and (2) radiative or far-field region. For wireless charging of electric vehicles, only near-field technologies are used. Near-field means the energy remains within a small region of the transmitting system. The range of these fields depends on the size and shape of the transmitter and receiver. In the near-field region, the electric and magnetic fields can be studied separately. A power can be transferred through the electric field via electrodes and the

CONTACT Lionel Pichon lionel.pichon@geeps.centralesupelec.fr Group of Electrical and Electronic Engineering of Paris, Université Paris-Saclay, CentraleSupélec, CNRS, Paris, Gif-sur-Yvette 91192, France; Group of Electrical and Electronic Engineering of Paris, Sorbonne Université, CNRS, Paris, Gif-sur-Yvette 75252, France

magnetic field via coils. Power decreases with a $1/r^3$ factor, where r is the distance from the source, and then energy remains at short distance between the transmitter and the receiver.

The capacitive power transfer (CPT) is dual of the inductive power transfer (IPT) technology. The IPT system uses magnetic fields to transfer power, while the CPT system uses electric fields. The CPT system has several advantages: negligible eddy-current loss, low cost and weight, and good misalignment performance. In a CPT system, only several pieces of metal plates are used to build the capacitive coupler. There is no issue about the eddy-current loss. The material and thickness of the plates do not affect the system performance very much. The CPT system is able to transfer power across electrically isolated metal barriers. Capacitive power transfer can be used in various applications, such as integrated circuits, biomedical devices, personal electronic devices and electric vehicles (EVs). The capacitive interface is typically in the range of hundreds of picofarads (pF) when the plates are almost touching with an insulation layer in between and 1–2 mm air gap, and few tens of picofarads. For EV charging applications with a large air gap (from 150 to 300 mm), the frequency is around 1 MHz.

The inductive Power Transfer-Based Wireless Charging (IPT) uses the principle of magnetic induction to transmit power without a medium. It is based on Maxwell's law, where a time-variant current in a conductor creates a magnetic field around the conductor, and a secondary loop (receiver) gets voltage generated due to time-varying magnetic flux. The disadvantage of such inductive coupling technique is that efficiency is lost as fast as coils are separated. Therefore, the non-resonant method is no efficient for long distances leading to waste more energy when transmitting over longer distances.

Mechanical resonance (or acoustic resonance) is well known in physics and consists in applying to a system a periodical action (vibratory motion for example) with a period that matches the maximum absorption energy rate of the system. When two systems have the same resonant frequency, they can be coupled in a resonant way leading one system to transfer energy (in an efficient way) to the other. In electromagnetics, the resonance is needed to improve efficiency drastically by transferring the electromagnetic energy to the receiving coil resonating at a matching frequency. Thereby increasing the charging distance as compared to other methods. It is important to note that due to resonance characteristics, power is only transferred to object operating at a matching frequency and has no effect on objects with nearly matching frequency. When the electric vehicle is parked at a fixed place, electric power is transferred from the pad underneath the ground to the one mounted on the chassis of the vehicle with any contact with each other. To transfer power in a convenient manner and productively, resonant compensation should be used to remove the great inductance leakage and the small coupling.

The present paper is devoted to a particular technology on the domain of WPT called inductive power transmission (IPT) and its application oriented to the charge of electric vehicles. The automotive industry is currently undergoing a major technological transformation in a context where environmental concerns are at the forefront. Restrictions in terms of CO2 emissions lead manufacturers to work on "cleaner" concept cars as the Electrical Vehicle (EV) and Hybrid Electrical Vehicle (HEV). Such vehicles currently use a regular cable connection for the recharge (on board battery) in charging stations. Although this kind of charging, developed in recent years, is known to be very fast (15/20 min) for full EV battery charge with proper energy, it may include elements tedious and/or inconvenient for the

user who deals with the charger cables that needed to be plugged in the station. In addition, the charging cable needs to be checked for maintenance and is not easy to handle. Tt may be dirty because of ground contact and it implies daily tedious movements. In this context, to avoid cables disadvantages, contactless charging (wireless charging), is an attractive alternative solution with more flexibility. In the short term, this technology, indicated as static as the vehicle is parked or stopped during the charge, will probably substitute the conductive systems. However, the absence of mechanical constraints is leading the possibility to use the inductive transfer during the motion of the vehicle toward the dynamic IPT. The installation of dynamic IPT systems into the road infrastructure will eliminate the necessity of stops for the recharge and, in the near term, this application could lead to a strong reduction of the on-board installed battery capacity. The success in the demonstration of the feasibility of this technology can indicate a practicable way to improve the electric mobility acceptance and solve the most critical aspects in the use of electric vehicles.

The overall system is made of two main parts: the contactless coupler and the power electronics system (Figure 1). Up to the wireless stage, there are two conversion steps: The low frequency AC from the grid is converted to DC, and then the DC to AC high frequency. These conversion stages allow adjusting the power level by controlling the input voltage and the frequency. After the wireless stage, a final conversion from high frequency AC to DC is done to provide energy to the battery. Depending on the application (static or dynamic) power levels typically range from 0.5 to 200 kW for a gap of 10 to 250 mm. The operating frequency extends from 20 to 100 kHz. Because of the large distance between the primary and secondary sides, the coupling is weak. In consequence, in order to reach the desired transferred power, high reactive power must be managed and the use of resonant elements in both sides is necessary as compensation to ensure good efficiency. Resonant converters are needed to compensate the inductive parts of the system and, on the other hand, improve

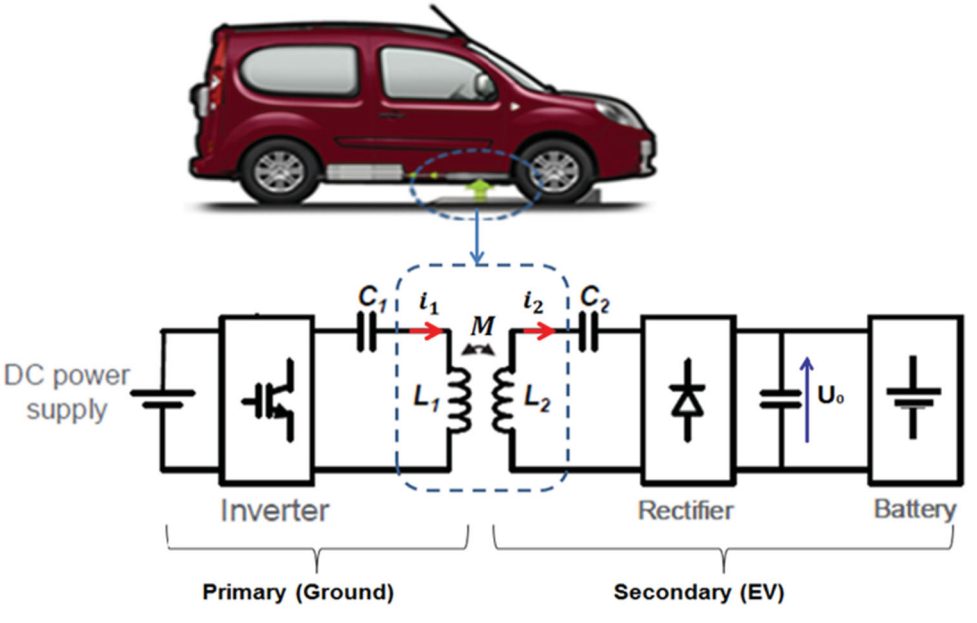

Figure 1. IPT charging system for electric vehicle EV.

the coupling of the magnetic link [2]. Several works highlighted the criteria of inductive compensation using series or parallel connections, and they made comparisons between them [3–5]. Also the output parameters at the load side should be regulated in order to keep the charger operating at a certain voltage with the desired current demanded by the battery. Furthermore, controlling the output parameters insures load protection.

The four basic compensation topologies are generally labeled as SS, SP, PP, and PS, where the first S or P stands for series or parallel compensation of the primary winding and the second S or P stands for series or parallel compensation of the secondary winding. It comes out from a comparison of these four basic topologies that SS compensation is the one requiring less copper mass [4]. From an economical point of view, SS and SP compensation are more advantageous for high-power transmission. For low power levels, PS and PP allow working at a larger distance with the same operating frequency. However, the value of the parallel capacitors depends on the load which is not a practical solution for one receiver coil application. So theoretically, SS is the best topology, as the primary capacitance is then independent of either the magnetic coupling or the load. The other three topologies are all dependent on the magnetic coupling.

This paper presents different electromagnetic considerations to take into account for the design of efficient coupling system. On the basis of recent work published in the literature and of the work performed in GeePs, the paper describes the electromagnetic aspects to tackle to improve the design and safety of inductive charging for electric vehicles. The paper is organized as follows. In Section 1, a state of art regarding inductive charging for electric vehicles is summarized. Section 2 illustrates the need for an accurante 3D electromagnetic analysis of the coupling system in order to deduce electrical parameters. Also the need for interoperability is illustrated. Section 3 addresses the human exposure problem with reference to international recommendations due to the high power driven by the system. In section 4 is described a way based on surrogate models, to manage uncertainty in various parameters involved in the global electromagnetic problem. Finally, a conclusion underlines the key features of this challenging field and suggests several ways to go further.

1.1. Historical aspects and state of art

This summarized historical review is extracted from [6]. Some recent papers also address the state of art in this field [7–9].

The first real improvement comes with Tesla studies. Tesla invented the definition of wireless power transmission [10,11] and demonstrated the feasibility of a first example of contactless transmission at the Universal Exposition in Chicago in 1893. Seven years later Tesla obtained a patent. for a long distance wireless transmission system for which he highlighted two important cornerstones of inductive transmission:

- The need to operate at higher frequencies due to the large distance between the coils
- The use of capacitors connected to the coils in order to work at the resonant frequency improving the efficiency of the transmission.

A first real application of the inductive transmission arrived from the soviet electrical engineer Georgiy Babat. In 1943 Babat built an electric car, named HF automobile supplied

through IPT. The system was composed by copper tubes forming a series of path buried under the asphalt and a receiver placed under the vehicle at about 20 cm from the ground. The system was supplied through an electron-tube oscillator [12] providing a current of hundreds of ampere with a frequency of 50 kHz. The induced current was rectified and used to directly supply a 2 kW motor. This first prototype had only 4% of efficiency but it was the first working implementation of an IPT system for electric vehicles.

The first system adopting solid state devices appeared in a patent deposited by D.V. Otto in 1974 [13]. Otto proposed an IPT system for an electric vehicle supplied through a silicon controlled rectifier inverter currying a current of 2000 A at 10 kHz. In this case the resonance of the receiver was assured through a series connected capacitor and connected to a DC motor by means of a rectification stage. The work was abandoned in the same year. In the 1980s, a first working IPT system with a moving vehicle was designed within the project PATH in California [14]. The goal of the project was the development of a segment of electric roadway to inductively power a small electric bus. The system operated with a variable air-gap between 5 and 10 cm and provided a power of 200 kW through a maximum current of 2000 A generated by an electrical machine working at the fundamental frequency of 400 Hz. The particularity of this prototype was the way to control the power transmission as variable capacitors were employed to detune the receiver resonant frequency. The achieved efficiency was of about 60%, but the prototype presented different critical aspects such as the huge dimensions and weight of the coils: the receiver was 4.5 m long and 1 m large with a weight of 850 kg.

In the 90s the massive interest of researchers and industries on the IPT technology started according to the improved performances of the power electronics devices at frequencies above the tens of kHz with currents between tens and hundreds of amperes. At the end of the last century the diffusion of IPT systems for the charge of hybrid and electric buses began.

In 1997, the german Wampfler AG, implemented a first commercialized IPT system for public transport based on the patents developed by the Auckland University [15,16]. This system was conceived to charge stationary buses and the technology named static IPT. The system planned the alignment of the receiver through a camera placed under the vehicle floor and the subsequent swiping down of the receiver obtaining a gap of about 4 cm respect to the buried transmitter. Electric buses wirelessly charged during parking, in an automated fashion, operate in Genoa and Turin since 2002. The Wampfler system operates at a frequency of about 15 kHz with a rated current of 80 A transmitting a rated power of 30 kW. The small air-gap between transmitter and receiver guarantees a good magnetic coupling and reduced stray fields level.

Over recent years several companies and research centers have proposed their systems to improve the electrical mobility through the IPT. WAVE, a startup born within the Utah State University, commercializes its IPT technology for the recharge of the electrical buses. The first demonstration prototype has been implemented in a campus shuttle equipped with a receiver having the same dimensions of the transmitter embedded in the pavement of the bus stations. This system allows the transfer of 25 kW at 20 kHz at each bus stop. The transfer takes place over an air-gap of 15-25 cm obtaining an efficiency of 90% [17].

Since 2015, the implementation of the PRIMOVE IPT system for electric buses, provided by Bombardier is ongoing in the cities of Mannheim and Berlin (Germany) and in the city of

Bruges (Belgium). The presented solution works during the bus stops transferring a power of about 200 kW [18].

For of dynamic IPT, the Shaped Magnetic Field In Resonance (SMFIR) system is developed by the Korea Advanced Institute of Science and Technology (KAIST) since 2009. The SMFIR concept is based on the use of a massive quantity of ferrite to force the flux to come across a defined path. This concept was applied to the OLEV (online electric vehicle) bus in 2011 and, currently, two OLEV buses are active in the KAIST campus in the cities of Daejeon and Gumi, both in South Korea [19]. The system is composed by a roadside power conversion stage that rectifies the power received by the electrical network and supplies the buried power tracks (i.e. transmitters) at a frequency of 20 kHz. The road embedded power tracks are installed in sections of 122.5 m in length and each section is divided into segments whose length can range from 2.5 to 24 m [19]. A system of complex active and passive shielding solutions are installed on the bus with the purposes of confining the magnetic field along the desired path improving the electromagnetic compatibility (EMC) and reducing the electromagnetic field (EMF) emissions. For shielding, a series of copper twisted brushes is used to create a closed conductive shielding path [20]. KAIST developed different versions of OLEVs reaching a maximum power transfer of about 200 kW with an efficiency of 74% [21].

On the automotive sector, in 2011, Qualcomm acquired HaloIPT, a New Zealand company spun o by the University of Auckland. The HaloIPT developed IPT solutions in a power range between 3.3 and 20 kW and in 2011 it became partner with Rolls Royce which proposed the IPT technology to charge the luxury Phantom EV. A spin off of the Massachusetts Institute of technology (MIT), WiTricity, that develops wireless power transfer systems for various industries and applications, proposes also a solution for the static IPT. Several systems have been proven to be functional but are not yet commercially available. However, Toyota has licensed the WiTricity wireless system and started trials and verification tests for their electric and hybrid models. Another product available is the Plugless Power, a 3.3 kW IPT stationary charger developed by EVATRAN and commercialized in partnership with Bosch. It consists of a system adaptable to each EV model with a transmitter side composed by a control panel containing the power electronics directly linked to the electrical LV network and a transmitter pad that can be placed on the floor. The Plugless Power were successfully tested with the Chevrolet VOLT and the Nissan Leaf EVs [22].

Several major worldwide projects have recently been led for static and dynamic charging. Prototypes have been studied for cars and light commercial vehicles. An exhaustive list of all main projects is out of scope of this paper. Summaries of major IPT systems and companies/universities with the corresponding electric and electromagnetic characteristics may be found in [6–8].

2. Electromagnetic considerations in WPT systems

2.1. Magnetic coupling system

The magnetic coupling structure is the key part of WPT system. A standard structure consists of two main parts: the contactless coupler and the power electronics system connected to it. Before the wireless stage, there are two conversion steps: The low frequency AC from the grid is converted to DC, and then the DC to AC high frequency (Figure 1). These conversion

stages allow adjusting the power level by controlling the input voltage and the frequency. Behind the wireless stage, a final conversion from high frequency AC to DC is done to provide energy to the battery. Because of the large distance between the primary and secondary sides, the coupling is weak. As a consequence, in order to reach the desired transferred power, high reactive power must be managed and the use of resonant elements in both sides is necessary as compensation to ensure good efficiency. Also the output parameters at the load side should be regulated in order to keep the charger operating at a certain voltage with the desired current demanded by the battery.

The coupling system which depends on the magnetic field induction ensures galvanic isolation between the source and the load. To improve the coupling between the coils some additional material is used to increase the mutual inductance by increasing the magnetic flux between the coils. Ferrites are generally used because they are almost loss-free at frequencies up to several hundreds of kHz, even for the lowest cost materials. Thanks to this magnetic circuit, induction is mainly concentrated between the two coils which helps in improving the coupling. Many shapes of coils can be chosen for both the primary and secondary parts: circular, squared, elliptical coils etc. The circular geometry is the most used in EV applications but a rigid core increases the system fragility and cost. In [23], the circular geometry was studied and core was fractionated in order to optimize the use of ferromagnetic material. Many configurations were simulated and was determined, due to physical feasibility, that a core composed by eight bars had almost the same performance has the geometry with the full core. The double D (DD) geometry appeared also rapidly and has a promising alternative to the circular geometry due to the better tolerance to misalignments and dimensions/power ratio [24] (Figure 2).

Sometimes other materials (like aluminum) as in Figure 3 that cover the ferrites, which in particular cases can also decrease the leakage flux, and act as additional shielding [25,26]. This solution is expensive, increases the weight embedded in the EV and may generate additional losses at high frequencies because of the aluminum resistivity. However, in a real configuration, the presence of the EV chassis above the inductive coupler can also be considered as an additional shielding with respect to people or devices being inside the car.

The fabricated coils usually used in this application are made of isolated Litz wire, for which skin and proximity effects are very small in the considered frequency range. In general, primary and secondary coils are designed at the same time in order to reach given performances of the whole system.

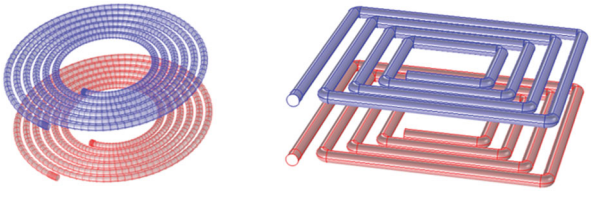

a) b)

Figure 2. Typical coils for inductive power system (a) circular type (b) rectangular type.

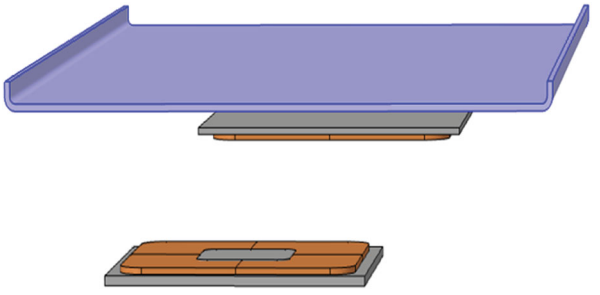

Figure 3. Rectangular system covered by shield [26].

2.2. Human exposure aspects

The coupling between the transmitter, which is placed on the ground, and the receiver, which is placed under the floor of the vehicle, leads to a large gap. This large space implies a high level of stray field near the coils, which can pose a problem of exposure to magnetic fields for passengers or persons likely to approach the vehicle during charging operations. It is therefore necessary to evaluate the level of exposure in order to comply with international safety instructions and to initiate research efforts to wireless charging systems and the human body.

Safety guidelines on electromagnetic field exposure are developed by several scientific committees of national and international organizations. The most prominent of these organizations are the International Commission on Non- Ionizing Radiation Protection (ICNIRP) [27,28] and the Standards Coordinating Committee 28 (SCC28) of the IEEE [29]. These committees continually monitor the scientific literature to derive exposure limits based on effects which the scientific community regards as established. These limits are issued in guidelines that are revised regularly. International guidelines for human exposure safety (such as ICNIRP 28) include two recommendations: reference levels and basic restrictions. The first recommendation to be checked is the reference level. If the reference level is exceeded, then a dosimetry analysis (involving the human body) has to be performed in order to be compliant to the guidelines.

3. Electromagnetic analysis of the coupling system

The WPT device has to be designed carefully. Basically, a magnetic coupling systems involves three main parts: coils, ferrites (ferromagnetic materials) and shields (conducting materials) The introduction of magnetic cores (high permeability, low losses materials) in the vicinity of the transmitting and receiving coils improves the mutual inductance and then the efficiency. The amount of the magnetic core has to be made as small as possible to reduce the cost and size without decreasing the efficiency. The magnetic core is usually designed considering these factors. Several shapes have been proposed in the literature: bar-shaped and H-shaped magnetic cores for example. In addition, the design of the transmitting and receiving coils is also very important for the efficiency of the system. For this reason, several types of coils with, for example, double -D, double -DQ, and circular

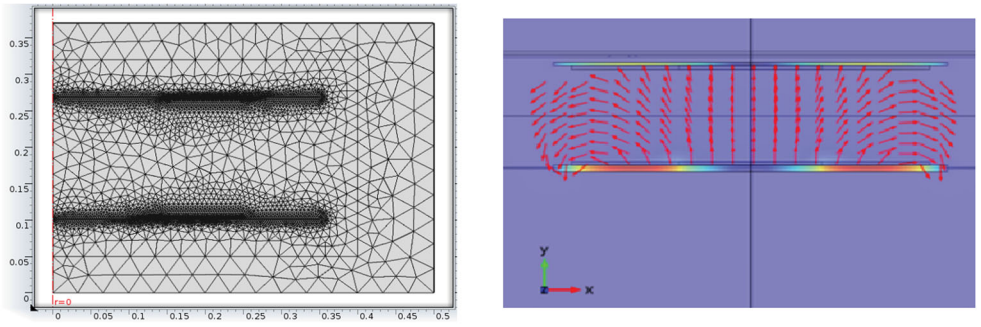

Figure 4. Finite element mesh of a typical circular inductive power system and computed distribution of magnetic flux density vectors (cut plane).

shapes are used. Finally, shield panels reduce the stray field and help to comply with human exposure recommendations.

The eddy currents produced in the shield panels (copper or aluminum) generate a magnetic field opposite to the field produced by the transmitted coil. As consequence the total magnetic field is reduced and then the performances are degraded due to the power losses in the conductive shield. A magnetic shield may improve the efficiency of the wireless power transfer system and can also mitigate the field if it is adequately shaped. As a conclusion, using both ferromagnetic material and metallic shielding may face the challenge. For example, a ferrite sheet placed between the coils and the metallic shield can reduce the losses in the conducting shield which permits to keep the efficiency as in the case of coils with ferrites only.

The optimal design of magnetic coupling devices, with adequate shapes and materials, taking into account both the efficiency of the system and the maximum level of electromagnetic human exposure remains an open problem. Several works attempt to deal simultaneously with these two aspects and present novel approaches to limit the stray field without decreasing the efficiency. For example, in [26], on the basis of the distribution of induced currents, the authors propose a hybrid shield using an aluminum plate and a thin copper ring along the outer edge of the aluminum plate. This solution appears as a low loss cost-effective alternative to a classical aluminum shield.

To solve the corresponding electromagnetic problem equivalent circuit models or approximated analytical solutions of the electromagnetic fields are available but very limited [30,31]. For these complex geometries numerical methods are strongly required [32–38] (Figure 4).

3.1. Numerical modeling of a circular WPT system

In order to illustrate the electromagnetic modeling part, the IPT system studied in [39,40] is considered. The work was performed in the framework of a project including three industrial companies: RENAULT (RNO), SCHNEIDER Electric (SE), and Newtech Concept (NTC). The tested EV is a KANGOO fabricated by Renault. The 3D structure of the coupling system is depicted in Figure 5. It consists of a transmitter coil, a receiver coil and two ferrites plates that completely cover the coils. A steel plate which describes

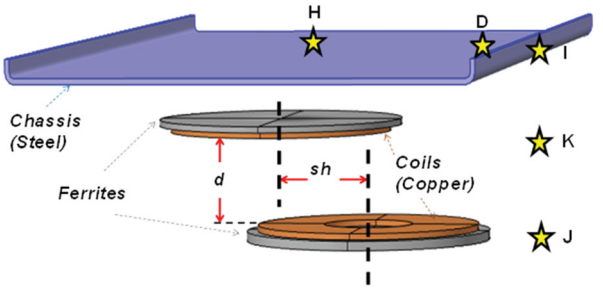

Figure 5. 3D structure with shielding, chassis and measurement positions (stars) for the magnetic field measures.

a simplified model of EV chassis is added in the design. The presence of the chassis has significant effect on the values of the inductances. It ensures better protection for the embedded electronic devices and reduces passengers' exposure to magnetic field.

Considering the range of frequency of WPT for electric vehicle (below 100 kHz), Maxwell's equations are generally solved in the frequency domain using a magneto-dynamic vector potential formulation (1):

$$\nabla \times (\mu^{-1} \nabla \times \vec{A}) + i\omega\sigma\vec{A} = \overrightarrow{J_e} \tag{1}$$

where $\vec{A}$ is the magnetic vector potential, μ is the permeability, ω is the frequency pulsation, σ is electrical conductivity and $\overrightarrow{J_e}$ is the current density.

The values of self-inductances L_1, L_2, and mutual inductance M can be then calculated from the magnetic energy using integration over the volume. To model the chassis by the finite element method (FEM), two cases are considered and compared:

- The chassis is made of a 5 mm width stainless steel ($\mu_r = 1000, \sigma = 10^6$ S/m) sheet. With the real characteristics the skin depth is very thin (~ 100 µm) at 30 kHz. For this case the element size in the finite element mesh size should be less than one third of the skin depth in order to have correct results with the FEM.
- The chassis is considered as a perfect electric conductor. Therefore, only the mesh of the outer surface of the chassis is considered.

The comparison between the two cases (with and without chassis) shows than no impact occurs on the values of the inductances and in order to alleviate the computational burden only the second case is considered in the following. Therefore, a 3D FEM modeling is performed considering the chassis as a perfect conductor. The calculation of the values of L_1, L_2, M includes the influences of variation of the parameters: d (distance between coils) and sh (shift between axis of the coil). Figure 6 shows the influence of d (m) variations at axis shift 0 and 0.1 m. It can be seen that the variations in the self-inductances L_1 and L_2 are large with a small air gap d, and they are small for large air gaps. This is because the ferrites and the chassis highly contribute to the magnetic flux distribution in the coupler for small air gaps. The mutual inductance M always decreases by increasing the air gap due to the

increase of the leakage magnetic flux and so the coupling factor k drops as shown in Figure 6. Because of the presence of chassis, the ICT is not symmetrical, and so $L_1 \neq L_2$ in general.

It can also be noticed that L_1 and L_2 do not have exactly the same variations with respect to *d* and *sh*. Without chassis these two inductances have the same value, this value varies with the position changes. The presence of the chassis leads to unsymmetrical magnetic field distributions for L_1 and L_2, and so, their inductances are different. The two values of these inductances vary independently with the position changes.

As an experimental validation for the developed model, a 2 kW power transfer for charging a 300 V_{DC} battery for the system in Figure 7 is carried out to check the $|B|$ levels at several points in the EV and the nearby environment (points *H, D, I, J* and *K* in Figure 5). The positioning parameters were taken as: $d = 10$ cm, $sh = 0$ and the switching frequency $f_s = 33$ kHz. The test takes the measurements of the magnetic field density $|B|$ as shown in Table 1 for a current $I_1 = 15$ A. All the points are under the maximum allowed magnetic flux density level for human exposure (6.25 μT considered in this work).

3.2. Parametric study of geometry

The EV chassis shown in Figure 5 with dimensions (1.6 m × 1.6 m) is used to represent the effect of the real chassis for a KANGOO RENAULT. In order to design efficient magnetic coupling systems for smaller vehicles, 2 simplified chassis are considered, with dimensions

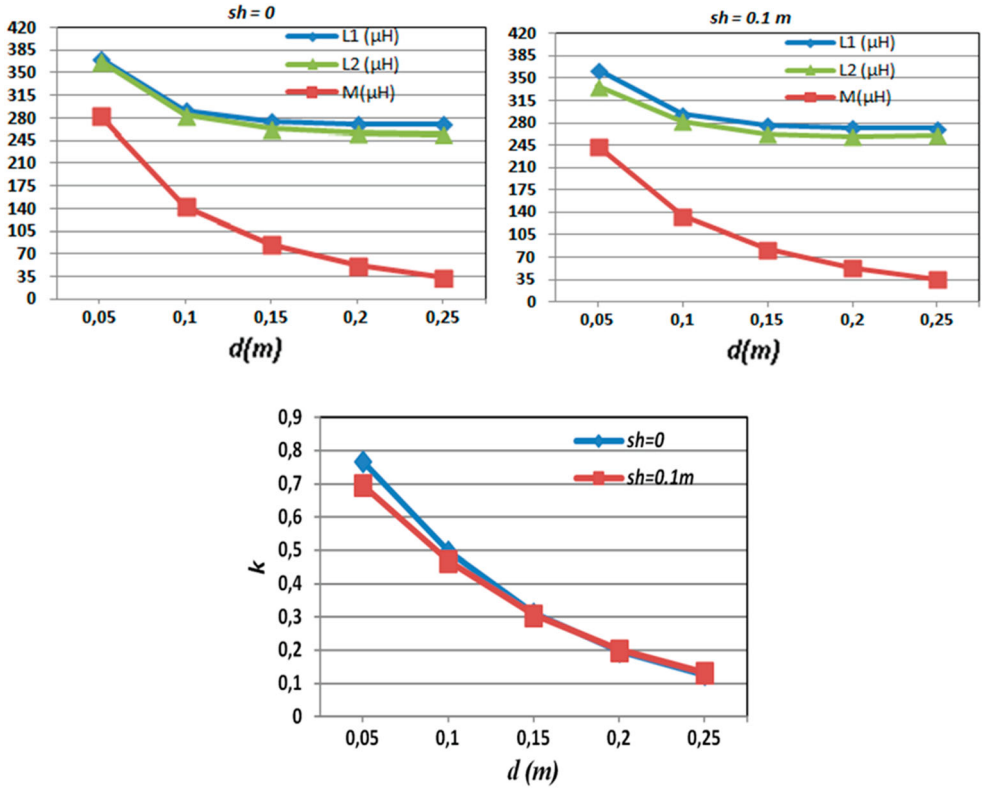

Figure 6. Values of L_1, L_2, *M* and *k* due to variation of air gap *d*(*m*) for $sh = 0$ and 0.1 m.

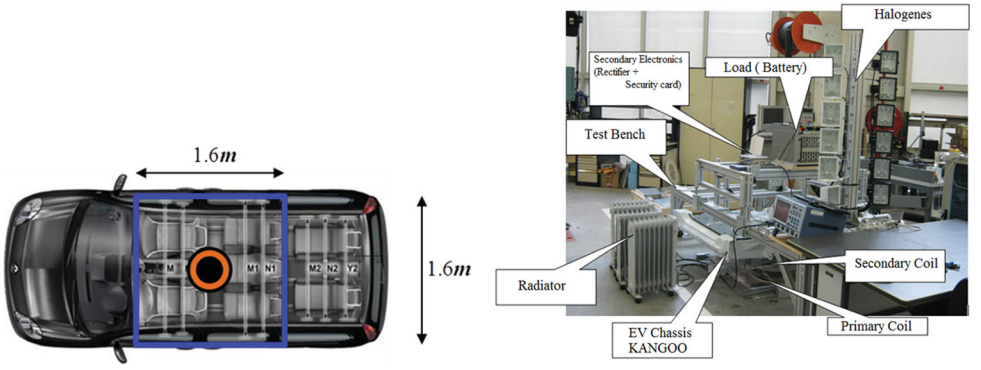

Figure 7. Experimental validation with a chassis of Renault KANGOO.

Table 1. Magnitude of the magnetic induction.

Parameter	Measured	Simulated
Point *H*	0.601 µT	0.002 µT
Point *D*	1.932 µT	1.876 µT
Point *I*	4.130 µT	4.800 µT
Point *K*	4.840 µT	5.010 µT
Point *J*	4.690 µT	4.650 µT

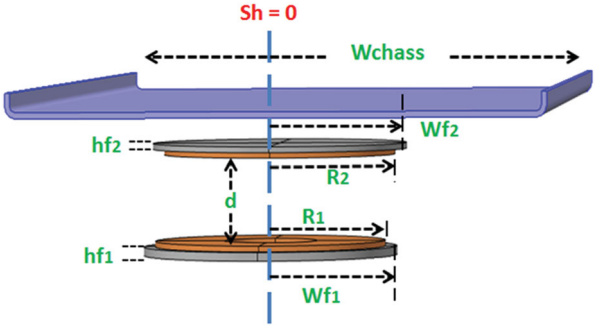

Figure 8. Parameters of the WPT structure with simple EV chassis.

(1 m × 1 m) and (1.2 m × 1.2 m). Some parameters of the system are fixed: the secondary coil radius is $R_2 = 150$ mm and the resonance frequency is $f = 30$ kHz. The aims are to find the primary radius R_1 which makes the coupling factor k maximum for the case that $sh = 0$ and to ensure that the radiated field complies with exposure standards $|B| < 6.25\ \mu$T. In this study, the ferrites for each case have a permeability $\mu_{rF} = 2000$ H/m, and the other parameters of coils and ferrite dimensions in Figure 8 are chosen as: $s_1 = s_2 = 112.5 \times 5.7\text{mm}^2$, $n_1 = n_2 = 15$ turns, $h_{f1} = 10$ mm, $h_{f2} = 3$ mm, $W_{\text{chass}} = 1$ m.

In order to achieve the wanted maximum value of k, the primary radius R_1 is parameterized and for each value of R_1, the value of L_1, L_2 are calculated, and finally k is computed. These values of k are plotted with respect to the ratio of R_1/R_2 as shown in Figure 9. It is clearly shown that the curve is maximized at the ratio of 1.5 between the primary coil radius to the secondary one. This is true for this specific configuration. However if other parameter

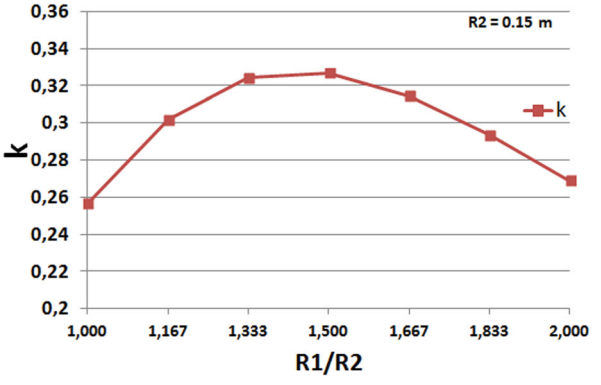

Figure 9. Plot of k in function of the parameterized norm $\frac{R1}{R2}$.

variations are considered, then the curve in Figure 6 will change and the maximum point also, but this change is weakly affected by the width of chassis (i.e, $W_{\text{chass}} = 1.2$ m).

3.3. Interoperability analysis

The interoperability study is a major point in wireless charging [41–44]. The term "interoperability" should be understood as the ability for a primary (ground) system and a secondary (board) system that were "independently" designed by different manufacturers to work together and insure battery charging. In the project considered above, different power pads are used to construct the coupling system [42]. The goal is to check the ability of different systems to work together. As there are three power pads (RNO, SE, NTC), a combination between two of them is performed to build the ICT. Here, four interoperability configurations are studied: NTC–RNO, SE–RNO, SE–NTC, and RNO–NTC. Any other combination can be also implemented like: NTC–SE or RNO–SE, but in this paper, the SE power pad takes a place only in the primary side (ground). The other two pads can be in the primary side or mounted in the secondary side (EV). The specifications of each power pad are illustrated in Table 2, and the considered interoperable combinations are shown in Figure 10.

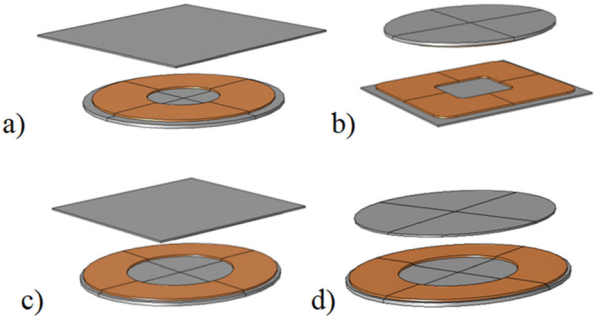

Figure 10. Interoperability prototypes: (a) RNO-NTC (b) NTC-RNO (c) SE-NTC and (d) SE-RNO.

Two of the three pads have the same shape with different dimensions (RNO and SE), and two of them have different shapes (RNO and NTC). All of the prototypes are placed in the middle of the EV chassis (as shown in Figure 7), and a simplified chassis is considered to calculate the mutual inductance, self-inductances, and the coupling factor *k*. In order to check the capability of each interoperable prototype to exchange the power between its sides, a comparison is made. Here, all interoperable prototypes are taken into account including the prototypes for the same power pads (RNO–RNO and NTC–NTC). The comparison includes self-inductances, mutual inductances, and the coupling factor. The computations are made for different values of the air gap distance (*d*) and the shift (*sh*). The comparison between different prototypes is shown in Figures 11–14 for L_1, L_2, *M*, and *k*, respectively. From these figures, the following points can be underlined:

(1) For L_1: The biggest values are for NTC–NTC prototype, while RNO–RNO prototype has the smallest values for both configurations with and without axis shift. It can be noticed that all configurations that have the same system in primary reach the same value of L1 at high air gaps for both cases of axes shift. This is because the ferrites and the chassis highly contribute for small air gaps, and in contrary, they have no more effects at high air gaps. It is also noticed that for small air gaps, if the dimensions of the ferrites at the secondary are smaller than the dimensions of the primary side (SE–RNO and NTC–RNO), the primary self-inductance is reduced compared to cases where the secondary ferrites are wider (respectively, SE–NTC and NTC–NTC). This behavior is due to the presence of the chassis on the secondary side.
(2) For L_2: The biggest value is the SE–NTC prototype, while the RNO–RNO prototype is the smallest value for both configurations with and without axis shift. This is true for small

Table 2. Power pad specifications.

Power Pad	Type	Specifications	
RNO	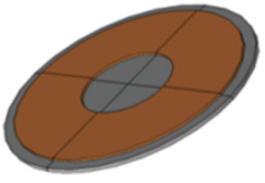	Coil	20 Turns Copper width 150 mm External Diameter 500 mm
		Ferrite	External Diameter 550 mm
SE	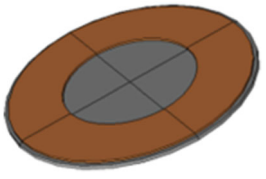	Coil	18 Turns Copper width 135 mm External Diameter 600 mm
		Ferrite	External Diameter 620 mm
NTC	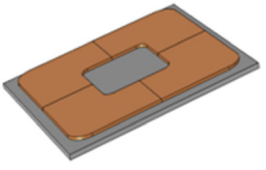	Coil	20 Turns Copper width 150 mm External width 500 mm
		Ferrite	External width 550 mm

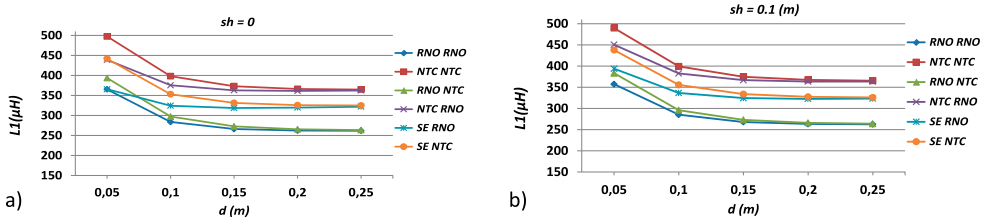

Figure 11. Values of L_1 for different prototypes as a function of the air gap distance d(m): (a) $sh = 0$ and (b) $sh = 0.1$ m.

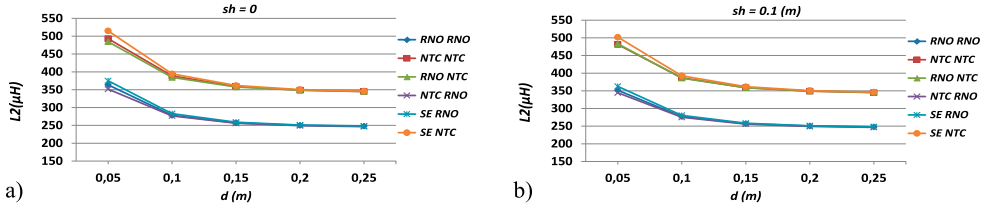

Figure 12. Values of L_2 for different prototypes in function of air gap distance d(m): (a) $sh = 0$ and (b) $sh = 0.1$ m.

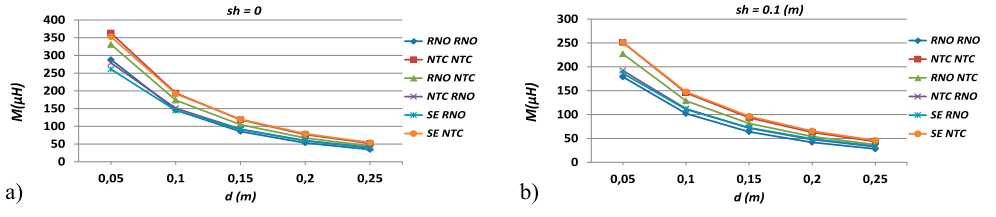

Figure 13. Values of M for different prototypes in function of air gap distance d(m): (a) $sh = 0$, (b) $sh = 0.1$ m.

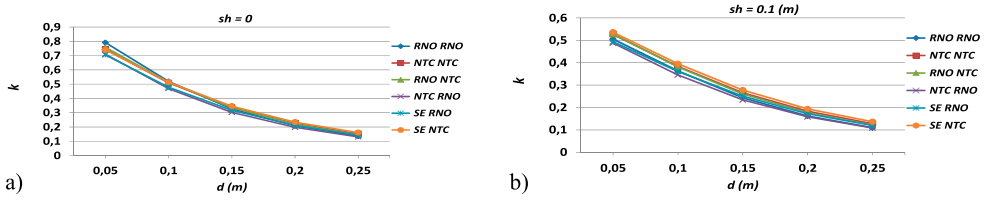

Figure 14. Values of k for different prototypes in function of air gap distance d(m): (a) $sh = 0$ and (b) $sh = 0.1$ m.

air gaps, but as the distance between the coils increases, the values of L_2 will converge for the configurations where the secondary pads are the same.

(3) For M: The best values of the mutual inductance M are NTC–NTC and SE–NTC prototypes. The weak values for small air gaps are of the SE–RNO prototype. With an axis shift, all M values of the prototypes are lower than the configuration without an axis shift. It can also be noted, as for the primary self-inductance, that the M value is

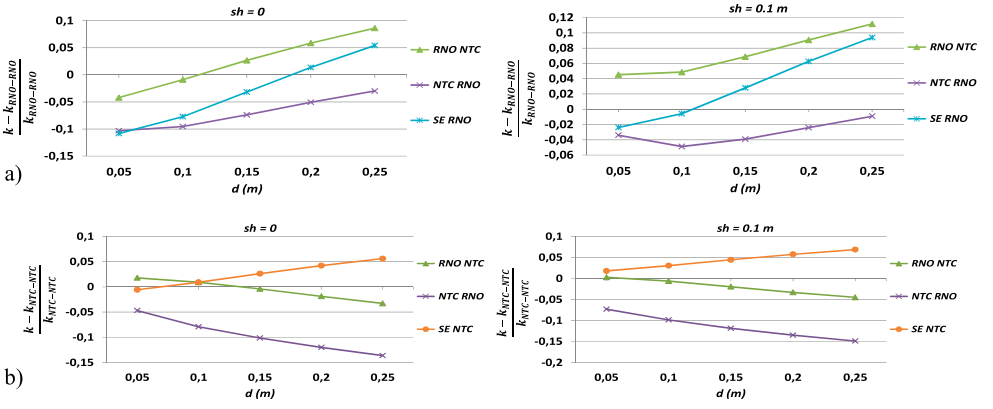

Figure 15. Comparison of relative difference of the coupling factor for two groups of reference prototype: (a) k_{ref}: RNO-RNO and (b) k_{ref}: NTC-NTC.

strongly reduced when the secondary side is reduced and gets smaller than the primary pad because of the effect of the chassis. For example, *M* (NTC–RNO) is smaller than *M* (NTC–NTC) and may even be smaller than *M* (RNO–RNO) when there is no axis shift. In fact, there are many factors that impact the value of *M*: the chassis, ferrites, flux cancelation phenomenon, and the effective area of the coils. So as the system is complex, it is difficult to draw general conclusion on the behavior of *M* value for each interoperability configuration. However, it can be noticed that when there are more ferrites, the *M* value will be stronger.

(4) For *k*: The coupling factors for all prototypes are closed to each other at high air gaps for the two configurations with and without axis shift. However, for small air gaps, and if there is no axis shift, the highest coupling factors are for the RNO–RNO prototype, while the smallest one is for the NTC–RNO prototype. In the other hand, where there is an axis shift, the high coupling is for SE–NTC and NTC–NTC prototypes, and the smallest coupling factor is for the NTC–RNO prototype. Moreover, the coupling factor values are smaller where there is an axis shift between the power pads of the different ICT prototypes. To illustrate the behavior of the coupling factor, two sets of interoperability configurations are studied separately with respect to the corresponding reference prototype. The first group includes the prototypes that have RNO pad either in the primary or secondary. The reference prototype of this group is RNO–RNO configuration. The second group contains the prototype where NTC pad exists either in primary or secondary. So the reference prototype for them is NTC–NTC configuration. The relative differences of the coupling factor for the two cases of study are shown in Figure 15. From this, it can be deduced that starting from a reference system for which the primary and the secondary are the same size, the configuration with a smaller secondary system will tend to decrease the coupling factor. However, contrary to that, the configuration with greater secondary will tend to increase the coupling factor (effect of the chassis).

In order to check the magnitude of magnetic field and the human safety compliance all the studied systems and in particular considering interoperability configurations,

Table 3. $|B|$ level values for different prototypes.

		SE-RNO		NTC-RNO		NTC-NTC		SE-NTC	
		Sim.	Measu.	Sim.	Measu.	Sim.	Measu.	Sim.	Measu.
POINT	*H*	0.2 µT	0.6 µT	0.2 µT	0.46 µT	0.2 µT	0.3 µT	0.2 µT	0.3 µT
	D	2 µT	2.2 µT	1.4 µT	0.82 µT	4.5 µT	3.65 µT	4.35 µT	3.4 µT
	I	4 µT	3.7 µT	3.8 µT	2.5 µT	3.5 µT	2.49 µT	3.3 µT	2.3 µT
	K	5.35 µT	5 µT	5 µT	3.7 µT	8.5 µT	7.08 µT	8.5 µT	7 µT
	J	4.3 µT	4.5 µT	4 µT	3.05 µT	4 µT	3.04 µT	4 µT	3 µT

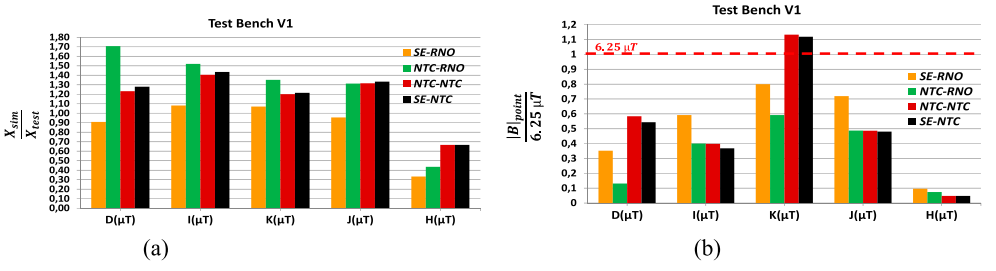

Figure 16. Comparison of values of $|B|$ levels of interoperability prototypes (a) simulation results normalized to test ones and (b) tests results normalized to 6.25 µT.

experimental tests are carried out (Figure 7) for (3 kW, 300 V) and ($d = 0.1$ m, $sh = 0$). The values of $|B|$ are given for the point shown in Figure 5. Table 3 includes the measurements of $|B|$ levels at the points (*H, D, I, J* and *K*) for different prototypes for the input primary and output secondary currents ($I_1 0^\circ$, $I_2 90^\circ$respectively in rms values) at the resonant frequencies using a Magnetic Field HiTester 3470 HIOKI. To compare the results of the calculation with the experimental ones; the values are firstly normalized to 6.25 µT, and secondly the simulation values are normalized to the test ones. The results of comparison are illustrated in Figure 16(b). It can be seen that simulation results may significantly differ from the test ones as shown in Figure 16(a). A great part of this error is due to the lack of accuracy in the positioning of the magnetic field sensor. Actually the measurements were done manually using the sensor, the only point that marked in manipulation was *D*. So a difficulty was encountered to position the same point at each test. Moreover from it can be noticed that all values are under the norm except for the point *K* for the prototypes NTC-NTC, SE-NTC for both simulation and test results for same charging characteristics (3 kW, 300 V battery). Considering the interoperability, if one looks at the flux density at critical point *K*, it can be said that:

- Coupling systems having the same size in the considered direction (D-K) but different shapes do not significantly change the induction (SE-NTC versus NTC-NTC).
- Coupling systems of different sizes lead to an intermediate value of induction compared to the original systems (NTC-RNO versus NTC-NTC).
- It also can be drawn that as the flux density is concentrated in the ferrites, the relevant size to be considered in this analysis is given by the size of the ferrite, which in the studied systems is close to the size of the coils.

4. Evaluation of human exposure

With the expansion in the use of wireless charging systems by inductive power transfer (IPT) for electric vehicles, it is important to dedicate research efforts to interactions between the wireless charging systems and the human body. A large amount of research has been dedicated to the study of human exposure to EM environment, e.g. handset antennas and wireless resonant power system [45–47]. However, in the frequency range of inductive power transfer for electric vehicle, the study of human exposure remains a crucial issue. For such an objective representative human models and adequate modeling methodologies have to be investigated.

4.1. Anatomical models

The dielectric properties of the tissues of the human body are varied and depend on the environment. They can be classified into two categories depending on whether the water content is high (muscle, brain, skin and internal organs) or low (fat and bone). At 10 MHz the relative permittivity of fabrics with a high water content varies approximately from 100 to 500 and their electrical conductivity from 0.15 to 1.5 S/m. For media with low water content the relative permittivity varies from 8 to 36 and the conductivity from 0.01 to 0.08 S/m. Below 10 MHz the dielectric parameters of nerves and muscles are anisotropic [48]. The absorption of the human body can be assessed relatively correctly using simple geometric shapes to represent the human body [49]. The evaluation of the local SAR requires a good knowledge of the anatomical characteristics. In addition, the posture of the body should be considered because it can significantly modify local absorption, especially when curls are formed with the arms, legs or fingers. Elements concerning the generation and description of human body models can be found in the literature [50–59]. Only the most recent models are independent of the mesh according to the resolution and the orientation in the field of computation. Also some models incorporate articulated limbs or have variable masses [56].

4.2. Numerical dosimetry

Historically the finite difference method in the time domain was the first approach to be used for digital dosimetry calculations [60–62]. As it is based on the use of a Cartesian mesh, its application to complex geometries such as the human body remains delicate. Applications related to low frequency inductive charging require the use of a large time step in order to guarantee the stability of the method. In addition, the resonant nature of the system leads to long simulation times to reach the steady state. Some approaches dedicated to tackle this problem in the framework of the generalized FDTD (Finite Integration Technique) has been proposed in [63].

The finite element method, generally used in the frequency domain exploits a spatial discretization in the form of tetrahedra. The ratios between edge lengths of the tetrahedra should be limited to avoid numerical errors. The wavelength associated with inductive charging systems is several tens of meters, which is why a quasi-static approach is justified. Quasi-static approaches have been implemented for the finite element method in the case of regular grids [64,65]. The dominant coupling is due to the magnetic field. The latter is hardly affected by the presence of a human body. Consequently, the magnetic field produced by the system can be studied independently and determined by an appropriate

free space method. These "incident" fields can then be applied to predict dosimetric quantities in the presence of the human body. An anatomical model can therefore be placed in the region where these so-called "incident" fields exist (fields due to the source).

4.3. Shielding

The EMF emission depends on the power level and shielding effectiveness of the charging pads. An aluminum shield is commonly used in the transmitter and receiver to limit the EMF emission for a wireless system. The shield effectively suppresses the EMF emission above the receiver and below the transmitter, but it is comparatively less effective along the sides. Moreover, with the increasing demand for fast vehicle charging, the high power system is becoming a potential solution. However, at high power, the EMF emission at the concern areas tends to increase beyond the international regulations, and the system requires a highly effective low loss shielding.

Many works have recently addressed the evaluation of the stray field comparing to reference levels and evaluated in various configurations the induced field quantities in human tissues due to inductive power systems [66–71].

Therefore, there is a need for a comprehensive study to investigate the shield characteristics and to optimize the shield design for suppressing the EMF while minimizing the shield loss. This is a crucial point widely addressed in the literature [72–80].

4.4. Static analysis in case of a 3 kW power

To illustrate the human exposure, for example, in [81] it was shown that the field values deduced in the case of a homogeneous human body phantom placed near the realistic charging structure [39,40] respected the recommendations of the ICNIRP. This charging system is assumed to deliver 3 kW on a 400 V battery, which decides the distance between two coils. The operating frequency of this charging system is 30 kHz. For a general exposure configuration, the phantom, considered as a passenger, is designed to stand closed to the charging system, as shown in Figure 17. The nearest distance between the center of the coils and the body is 0.8 m due to the size of the chassis. Figure 18 shows the distribution of induced normalized magnetic flux density, normalized electric field inside the whole human body. It is worth noting that the magnetic flux density with the maxima 0.46 μT and E-field with the maxima 0.003 V/m inside the human body are much smaller than the corresponding general public exposure limitations (27 μT for B and 4.05 V/m for E). Figure 18 shows the EMFs distribution on the cutting surface at the x-z plane in the human body. The maximum of magnetic flux density is 0.18 μT and the maximum of E-field is 0.0012 V/m. It is observed that compared with the general public exposure guidelines (27 μT for B and 4.05 V/m for E), the results comply with the exposure limits very well. The results for this exposure configuration confirmed that the compliance of the representative wireless inductive charging system with electromagnetic exposure levels can be achieved, which means that the wireless charging system meets safety requirements in this case.

4.5. Dynamic charging

In the case of dynamic recharging, the various transmitters are energized for a few milliseconds when the vehicle passes, generating transient fields. For example, at 40 km/h the

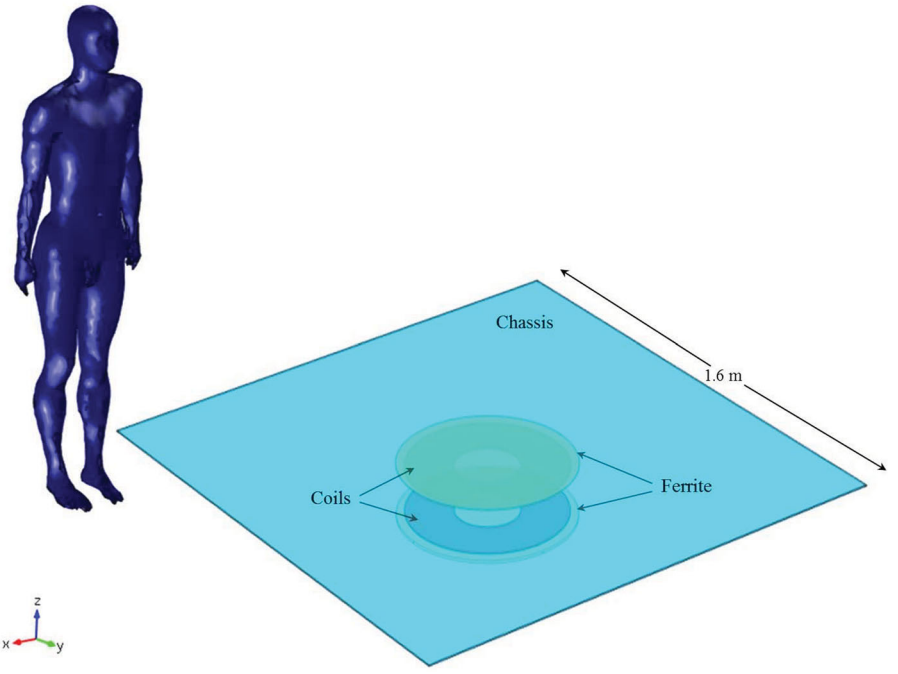

Figure 17. Human body model and representative wireless inductive charging system.

duration of the vehicle's passage over the transmitter is around 135 ms. The ICNIRP recommendations provide different methods for analyzing transient fields. The one adopted in the last recommendation is the weighted peak method (WPM) proposed by Jokela in [82] and introduced by the ICNIRP in 2003. The reader can refer to [6] for more details and a practical case. The key point is that the exposure can be assessed by means of a time-harmonic formulation for the range of frequency considered in inductive power systems [83].

The exposure assessment in the dynamic case must integrate the possible offset between transmitter and receiver. This is the case, for example, when the vehicle stops temporarily and someone is nearby. The distribution of the mutual inductance value depends on the offset between transmitter and receiver. As shown in [6], for distances between coils greater than 15 cm, the chassis of the vehicle has no effect on the coupling. The worst-case in terms of exposure is determined by calculating the induction in the volume shown in Figure 19. For each offset value, we identify the maximum value of the induction in the volume and the number of points for which the value limit is exceeded. At the frequency of 85 kHz this limit is equal to 27 μT (ICNIRP 28). This procedure makes it possible to define the worst case not only by considering the conditions which give rise to the maximum induction but also those which have the largest volume in which the values of the induction exceed the limits. When the worst-case situation is identified a dosimetric analysis can be conducted to assess the electric field in the human body. This analysis is carried out in [83] by the Duke model, (34 years old) from the Virtual Population family [50].

The study depends of course on the position of the receiver on the vehicle (center or rear). The rear position is the most critical since in this case the transmitter may not be completely covered by the vehicle. This situation results in an extension of the volume in which

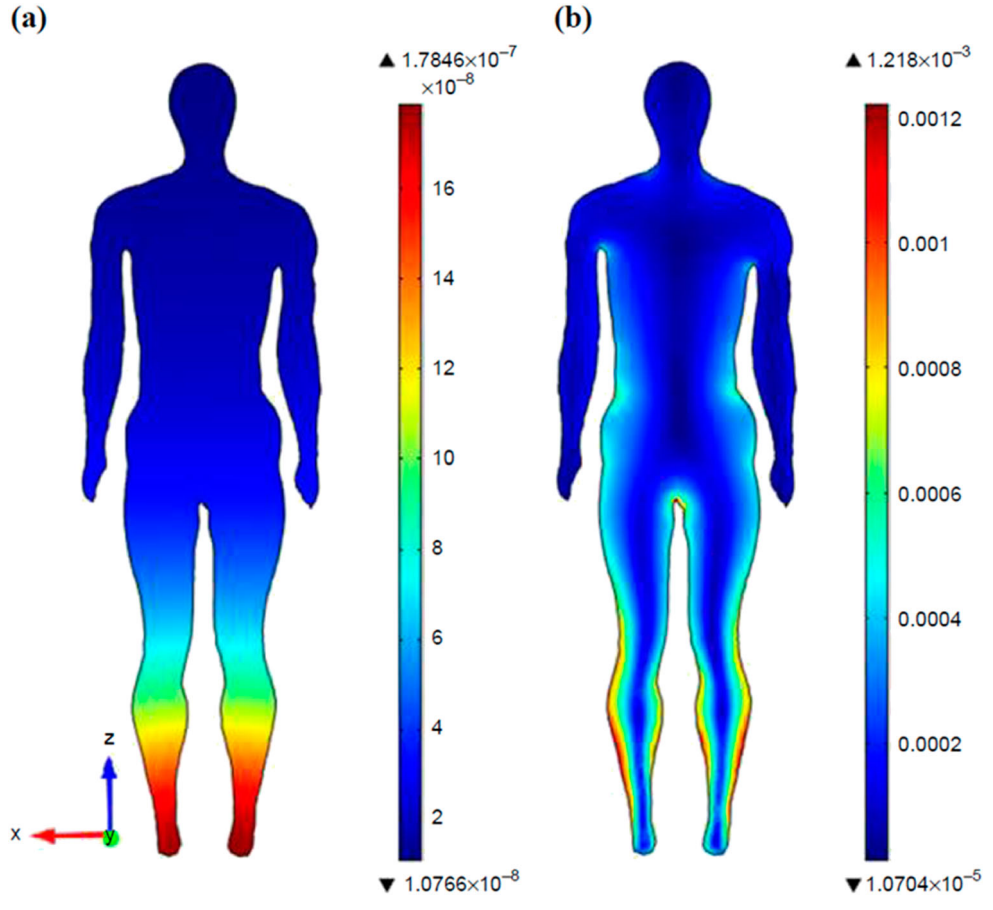

Figure 18. Distribution of induced EMFs inside the human body for the studied configuration. (a) Normalized magnetic flux density B (T); (b) normalized E-field (V/m).

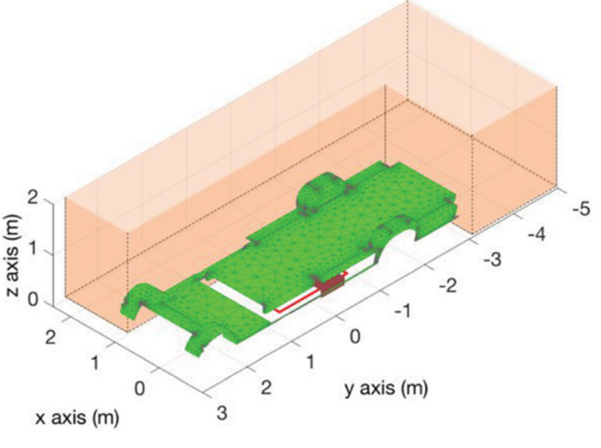

Figure 19. Region of electromagnetic field evaluation.

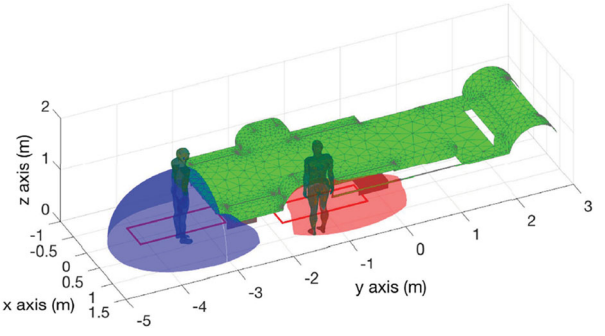

Figure 20. Boundary of the volumes having magnetic flux density higher than the reference level of 27 μT and position of the Duke model for the exposure assessment (blue: receiver on the rear, red: receiver on the center).

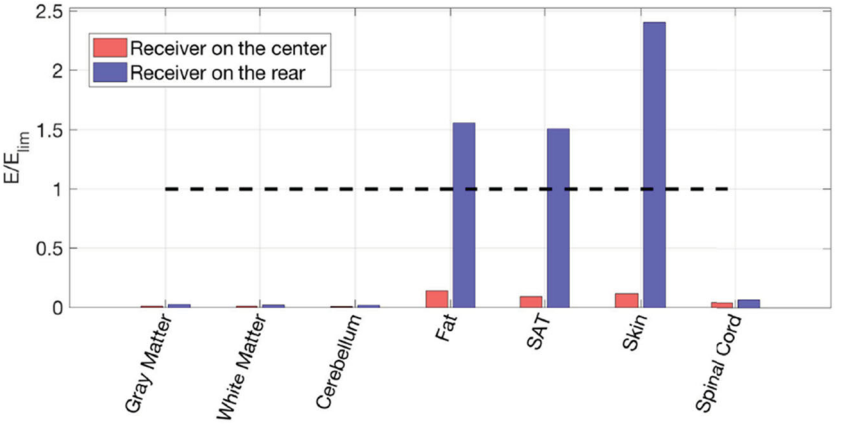

Figure 21. Exposure index on the selected tissues for the analyzed worst cases.

the limit is exceeded. The human body is then placed in the location corresponding to the maximum intersection between this volume and the body as shown in Figure 20. Figure 21 shows exposure indices for certain tissues. In this case the exposure is not in conformity (index $>$ 1) and therefore this provision is not advisable. A safety distance can then be proposed in order to protect people. As shown in Figure 22, this distance can be determined by considering the areas delimiting the volumes where the induction values are exceeded for different positions of the vehicle.

5. Uncertainty quantification

Previous sections have demonstrated that 3D electromagnetic modeling can improve the design of wireless power systems taking into account human exposure recommendations. However, it is also important to evaluate the efficiency of the system and the shielding effectiveness (SE) due to uncertainties in the electromagnetic and physical properties of materials; for instance, electrical conductivity of new composite materials have a strong impact on the shielding effectiveness of sheets. The properties of shields and magnetic materials used in such systems are very dependent on many parameters (thickness, number

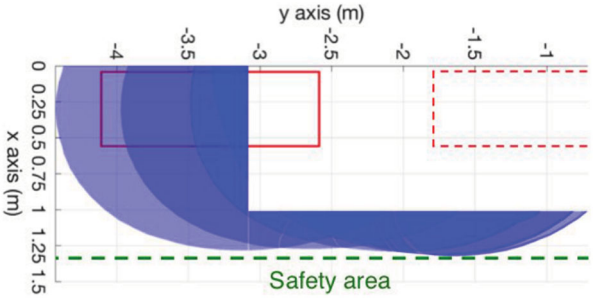

Figure 22. Definition of the safety area. Different volumes where the limit of *B* is exceeded in blue. Transmitters in red. The dashed one represents the subsequent not active transmitter. The dashed green line represents the border of the safety area.

of layers, electromagnetic properties, etc.) and these parameters are corrupted by many uncertainties (measurements errors, approximations) that may have a significant impact on the shielding effect and/or the global efficiency. More generally the field of electromagnetics applied to wireless power transfer, dosimetry and electromagnetic compatibility is constantly subjected to the management of variability and complexity of configurations.

To deal with uncertainty and variability, statistical methods based on Monte Carlo simulations may provide reliable results [84]. With such an approach, a large set of inputs are considered and many evaluations of a model response are needed. This leads to a heavy computational cost in case of complex system configurations. To avoid the computational burden and take into account a large variability of data, it can be very useful to build adequate metamodels (or surrogate models). A metamodel is an approximated behavioral model, obtained with a reduced set of input data, and whose behavior is representative of the original model for all data. Metamodeling is a well know procedure in reliability and uncertainty propagation in mechanics. It often relies on stochastic techniques (Kriging, polynomial chaos expansions). In electromagnetics, similar approaches have been developed in electromagnetic compatibility problems [85,86] and human exposure evaluation due to extremely low frequency or radio-communications [87–90]. Recently the quantification of uncertainty relevant to electrical parameters of a simple wireless transfer system was studied using a polynomial chaos expansion [91]: both the transmitter and receiver units have simple shapes and only consist of a resonant coil (helical or spiral) and a matching loop. In [92] Kriging was combined with a finite element software for the design of an inductive power transfer system.

This section shows that a surrogate model based on polynomial chaos expansion (PCE) provides a powerful tool for optimizing the performances of the transmission link and perform a sensitivity analysis at low cost. In particular, such PCE gives straightforward results regarding Sobol's indices highlighting the most significant parameters in the study. This part extends previous work [93] where preliminary results dealing with the stray field emitted from an inductive power system were presented.

5.1. Polynomial chaos expansions

Polynomial chaos expansion methods are non-intrusive methods and use 3D solvers as black boxes [94]. Let *M* be a mathematical model that from *N* input values (parameters)

$x = (x_1, x_2, \ldots, x_N)$ generates the output (observable) y given by

$$y = M(x) \tag{2}$$

The input values maybe affected by some random variations or uncertainties. Assuming that the components of the input random vector X are independent, it can be shown that if the random response of the physical phenomena Y has a finite variance, then it can be expressed as an infinite modal expansion, denoted polynomial chaos:

$$Y = \sum_{\alpha} y_\alpha \Psi_\alpha(X) \tag{3}$$

where α is a multi-index, y_α are the coefficients, Ψ_α are basis functions, multivariate orthonormal polynomials. These polynomials are built using tensor products:

$$\Psi_\alpha(x) = \prod_{i=1}^{N} \Psi_{\alpha_i}^{(i)}(x_i) \tag{4}$$

where α denotes the N-uplet $(\alpha_1, \alpha_2, \ldots, \alpha_N)$ divided by subheadings.

These univariate polynomials are a family of orthonormal polynomials with respect to the margin probability density functions (pdf) given by

$$E(\Psi_k^{(i)}(X_i)), \Psi_j^{(i)}(X_i)) = \delta_{jk} \tag{5}$$

where δ_{jk} is the Kronecker symbol.

If $f_{X_i}(x_i)$ is the marginal pdf of the random input variable X_i, then from the independence of the input variables, the pdf of X is given by

$$f_X(x) = \prod_{i=1}^{N} f_{X_i}(x_i) \tag{6}$$

In case of uniform or Gaussian input distributions, the corresponding polynomial basis are the Legendre and Hermite polynomials families, respectively. The PCE coefficients can be estimated by using spectral projections or via the use of least-square regressions. The "projection" approach takes advantage of the orthogonality of the chaos polynomials.

A truncation of the Polynomial Chaos Expansion provides a surrogate model at low cost and allows the evaluation of the coefficients using least-square regressions. Let consider an approximate model $\tilde{M}$ of the exact model M. The corresponding random output $\tilde{Y}$ is given by a truncated sum of P polynomials expressed as

$$\tilde{Y} = \sum_{k=0}^{P-1} a_k \Psi_k(X) \tag{7}$$

The unknown coefficients of the truncation can be estimated through least square regression while minimizing a root mean square error. If we denote y the output vector collecting n values in the vector $y = (y^{(1)}, y^{(2)}, \ldots, y^{(n)})$corresponding to the n inputs $x^{(i)}$

($i = 1, \ldots, n$) given by $x^{(i)} = (x_1^{(i)}, x_2^{(i)}, \ldots, x_N^{(n)})$, then the estimated unknown coefficients derived from a regression approach are given by

$$\tilde{a} = \{\Psi^T \Psi\}^{-1} \Psi^T y \tag{8}$$

where Ψ is the matrix whose coefficients are $\Psi_k^i = \Psi_k(x^{(i)})$.

The Latin Hypercube Sampling approach, known as LHS, is often used for planning the design of experiments. The validation of the truncated model can be checked using LOO (Leave-one-Out) validation error. This last approach is a natural definition. If we consider n input values $x^{(i)}$ giving n output $y^{(i)} = M(x^{(i)})$, one sample point $x^{(j)}$ can be removed and a new surrogate model $M^{PC\setminus i}$ can be built on the basis of n-1 sample values. Then a comparison between the predicted output value with this surrogate model and the value $y^{(j)}$ can reflects the accuracy of the approach. This leads to the LOO criterion defined as

$$\text{LOO} = \frac{1}{n} \sum_{i=1}^{n} (M(x_i) - M^{PC\setminus i}(x^{(i)}))^2 / \text{Var}[Y] \tag{9}$$

From computational efficiency point of view, it is important to select the most important polynomials. The sparse polynomial chaos, based on least angle regression method and Least absolute shrinkage and selection operator method [95] (often used under the same "LARS"), are often used. They can be used to identify the polynomials having a significant influence on the sensibility indices and the statistical distribution of the output.

In order to identify the main important parameters, the "Sobol" decomposition [96,97] is a great interest. With this approach, the response of a process having finite variance and independent inputs can be decomposed into main effects and interactions, and the global variance can be decomposed into partial variances. Thanks to the orthonormality of the polynomial chaos basis, the global variance $\tilde{D}$ are the partial variances $\tilde{D}_{i_1,\ldots i_s}$ are given respectively by:

$$\tilde{D} = \text{Var}(\tilde{Y}) = \sum_{k=1}^{P-1} a_k^2 \tag{10}$$

$$\tilde{D}_{i_1,\ldots i_s} = \sum_{\alpha \in \tau_{i_1,\ldots,i_s}} a_\alpha^2 \tag{11}$$

where $\tau_{i_1,\ldots,i_s}$ is the set of α tuples such that only the indices $i_1, \ldots, i_s$ are nonzero:

$$\tau_{i_1,\ldots,i_s} = \{\alpha, \alpha_k > 0, \forall k = 1, \ldots, Nk \in (i_1, \ldots, i_s)\} \tag{12}$$

The indices given from the PCE are analytically obtained:

$$S_{i_1,\ldots,i_s} = \frac{\tilde{D}_{i_1,\ldots i_s}}{\tilde{D}} \tag{13}$$

5.2. Uncertainty quantification in the design of IPT systems

Three simplified but realistic configurations of wireless power transfer operating at 85 kHz are studied in this section. The first one was built in Politecnico di Torino [6,98], the second

one in GeePs [99] and the third one has been investigated in the framework of the European project MICEV [100,101]. All the calculations in this chapter are performed by the UQLab module in Matlab [102].

The first structure considered in this section contains two rectangular coils (the transmitter and the receiver), and two ferrite plates. This test case corresponds to an existing inductive power system that has been built in Politecnico di Torino, Italy. Preliminary results have been published in [98]. The design includes a steel plate that represents the chassis of the electric vehicle (Figure 23). The dimensions of the system are shown on Table 4. The relative permeability of ferrite is 2200 This system has been designed for dynamic charging but only static charging is considered in this study. The power electronics controls and keeps the rms value of the current in the transmitter at 36 A and the current in the receiver at 75 A.

In this example, the uncertainty regarding the frame conductivity, distance between coils and length of reception coil is investigated. Here, σ, d, L are the chassis conductivity, distance between coils and length of reception coil respectively. The range of variation is shown in Table 5. Regarding the conductivity, the range includes typical values relevant to composite materials which are used in automotive applications. These three parameters are important for such analysis since once a parking or a road is equipped with defined transmitter coils, different kinds of vehicle may be charged by the system (interoperability). The level of radiated field then depends on the type of the receiver system (L and d) and car body (σ). They may strongly vary according to the vehicle.

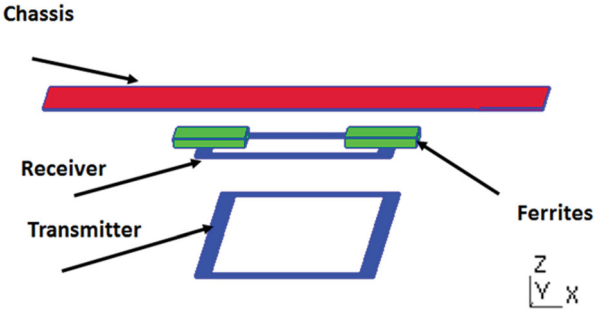

Figure 23. Studied configuration of the WPT system.

Table 4. Geometrical dimensions.

	Width (m)	Length (m)
Transmitter	0.5	1.5
Receiver	0.5	0.3
Ferrite	0.2	0.25
Frame	1.5	0.5

Table 5. Parameters: range of variations.

	8 points	10 points	15 points
LOO	2.2×10^{-3}	$1. \times 10^{-6}$	8.1×10^{-7}

Table 6. LOO values for different numbers of samples.

Parameter	Min	Max
σ (S/m)	10^4	10^6
d (m)	0.	1.
L (m)	0.2	0.3

For the studied case, the meta-model is constructed with 10 randomly selected data points out of 27 (3 samples for each of the three parameters). The electromagnetic modeling is performed with a finite element method (mesh shown on Figure 24). The computing cost for one simulation (three given parameters) is less than 2 min on a work station DELL XEON E5-1630 V3 (64 Go). The number of 27 data inputs points (full wave computations) is chosen as a compromise between accuracy and reasonable computing time in view of an engineering-oriented tool. The accuracy of the meta-model is then calculated on the remaining 17 points out of 27 to get the LOO. In order to study the influence of the number of samples on the predictions, the meta-models are constructed on 8, 10, 15 randomly selected points out of 27 data points. The values of LOO for different methods and for the three given cases are shown in Table 6. In practice it was shown that using more than 10 points is unnecessary to get a sufficiently accurate surrogate model.

The second inductive power transfer system (IPT) considered below has been studied in GeePs and is presented in [19] (Figure 25). There are two squared coils and rectangular ferrite plates. Starting from the equivalent circuit of the coupling system it can be shown that the power transfer efficiency can be expressed as [6]:

$$\eta \propto \frac{1}{1 + R_1 R_L / (\omega M)^2} \tag{14}$$

where ω is the angular frequency, R_1 is the series transmitter coil resistance, R_L is the series load resistance and M is the mutual inductance between the two coils.

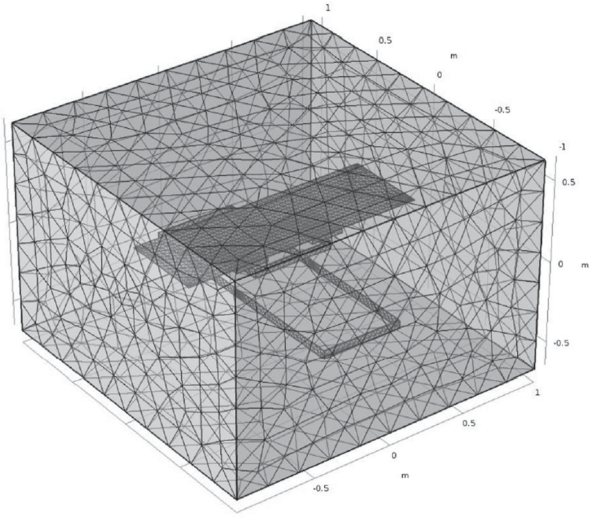

Figure 24. Finite element mesh used for computing sampling data.

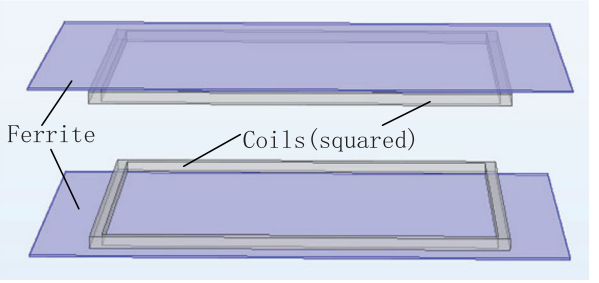

Figure 25. IPT system.

It is clear from Equation (4) that when the structure of the coils and the frequency of the IPT system are fixed, the efficiency is directly related to the mutual inductance.

The dimensions of the IPT systems are shown in Table 7. The design of the ferrites plates of a IPT system has a relatively strong effect on the power transfer efficiency. Here the uncertainty lies in the distance between the ferrite plate and the coil (d), the thickness of the ferrite plates (w) and the relative permeability (μ_r) of the ferrite material. A polynomial chaos expansions (PCE) is used to find the most influential parameters and to perform a first sensitivity analysis.

To illustrate, the metamodel is built with 120 samples, each sample including 3 values corresponding to the three parameters. The parameters are chosen uniformly distributed over the range of variations (Table 8). As Figure 26 shows, the LOO error rapidly decreases with the number of these datapoints. Around 20 datapoints is a sufficient number to obtain a value of M with less than 2% compared to the value computed with the 3D finite element model. To illustrate, Table 9 shows the quality of the prediction on the mutual inductance for some samples randomly chosen in the range of variations of the parameters.

In order to perform a sensitivity analysis regarding the mutual inductance M, the Sobol indices are determined and plotted versus the number of samples on Figure 27. It is clear that whatever the number of samples, the Sobol index for each parameter is nearly the same and the width of the ferrite plate is the most impacting parameter. Therefore, this parameter should be taken into account with great attention when designing the system.

Table 7. Dimensions of the IPT system.

Parameter	Dimension
Coil length	468 mm
Coil height	13 mm
Ferrite width	600 mm
Ferrite length	500 mm
Ferrite height	2 mm
Distance between coils	150 mm

Table 8. Parameters: range of variation.

Parameter	Min	Max
μ_r	1000	3000
d (mm)	0	15
w (mm)	0	2

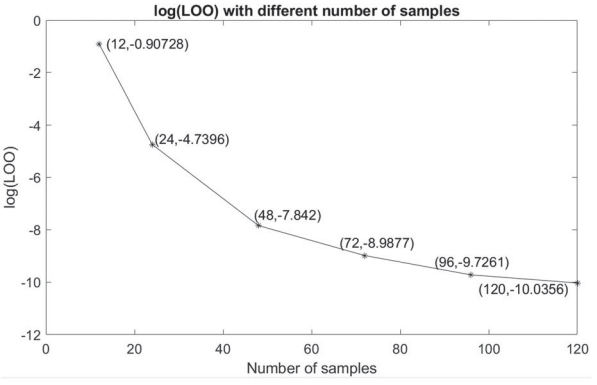

Figure 26. log (LOO) error versus different number of samples.

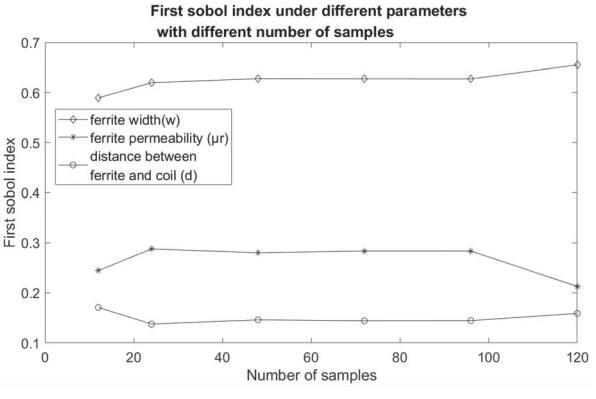

Figure 27. First Sobol index versus number of samples.

Table 9. Prediction on the mutual inductance.

Samples (w, μ_r, d)	M (FEM)	M (PCE)	Relative error
(1, 2000, 0.05)	9.33e−6	9.28e−6	0.0058
(1.5, 1500, 0.15)	5.91e−6	5.92e−6	0.0018
(2, 1500, 0.1)	8.04e−6	8.07e−6	0.0035
(2., 2500, 0.05)	9.94e−6	9.81e−6	0.0131
(1,1000,0)	9.33e−6	9.50e−6	0.0181

The third configuration is a light vehicle (Volvo sedan) which is studied in the framework of the MICEV project [100,101]. It is considered with three different positions for the coupling system: front, central and rear (Figure 28). The inductive power is 7.5 kW. The impact of physical parameters of the chassis and misalignment between receiver and transmitter on the B-field value in the surrounding of the vehicle are analyzed according to the physical properties of the car body. The range of variations of the relative permeability and conductivity are given in Table 10. The full wave computations performed by INRIM are used to build a metamodel based on 16 samples (4 values for each of the two parameters). The variation of LOO and the two Sobol's indices versus the number of samples is given in Table 11.

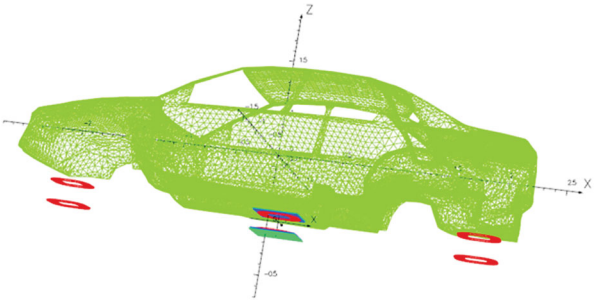

Figure 28. 3D mesh of the light passenger vehicle.

Table 10. Range of variation of the two parameters.

Parameter	Min	Max
μ_r	1	300
σ (S/m)	10	10^7

Table 11. LOO and Sobol's indices.

Number of samples	LOO	S_μ	S_σ
16	1.3×10^{-4}	0	0.99
10	2.2×10^{-3}	0	0.99
8	1.2×10^{-2}	2.2×10^{-4}	0.99
5	0.36	5.3×10^{-3}	0.98

To illustrate the predictions, Figure 29 shows, in case of $\mu_r = 200.$ and $\sigma = 10$ S/m the difference between the B-field predicted by the surrogate model (PCE) using only 8 samples and the B-field deduced from a 3D finite element computation [103]. Clearly in this case the surrogate model provides an excellent prediction.

As described above metamodeling may be used either to accelerate the numerical predictions while covering a wide range of parameters which affect the behavior of the system. The surrogate models could be used with a great efficiency in optimization procedures. As mentioned before the efficiency of the coupler has to be performed while keeping the constraints due international recommendations about to human exposure. Some first attempts regarding this objective [104–106] may be improved by using surrogate models or stochastic approaches.

6. Conclusion

The paper reviewed major challenges involving electromagnetic aspects of wireless charging systems dedicated to electric vehicles. Through several illustrative examples, the aim of the paper was to highlight three key features. The first consideration is to show that accurate numerical models able to deal with complex geometries and inhomogeneous materials are required to get reliable simulations that could serve as a basis for parametric studies in the design of efficient systems. The second challenge in WPT is to improve the

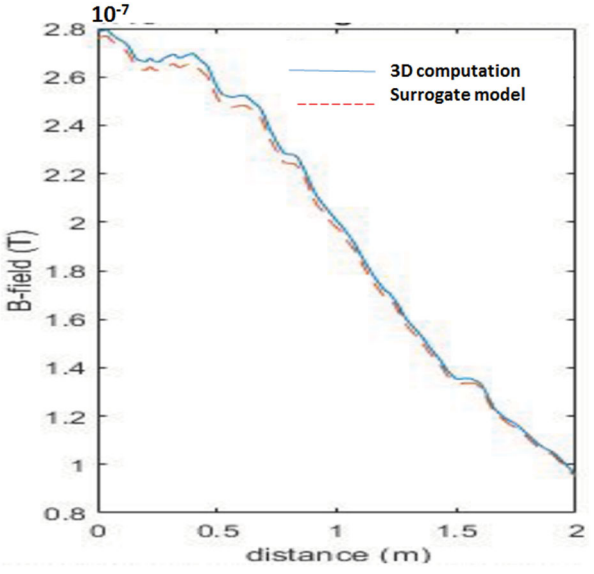

Figure 29. B-field on a vertical line located at 1.5 m from the side of the vehicle.

performances of the magnetic coupling system while reducing the stray field and keeping this value under the levels indicated by the international recommendations. For such an objective, complex electromagnetic analysis involving realistic human body phantoms need also to be achieved. Also new approaches dealing with appropriate active shielding provide a promising approach [107]. The third challenge relies on the capability to generate surrogate models, easy to use in optimization processes, able to deal with uncertainty quantification. Although computing power is still increasing, advances in the design of complex system (such as wireless charging systems) may benefit from these surrogate models: these behavioral models can provide major trends at low cost and identify the most significant parameters (geometry, materials).

Beside the engineering-oriented issues dedicated to design procedures and described in this paper, accurate costs evaluations from the economic point of view, are needed for a massive deployment of wireless charging technologies. The interoperability between different vehicles is also a key point that is now addressed with ongoing standardization processes. Even if dynamic wireless charging has been already validated on experimental representative roads [108], probably urban areas offer the most appropriate place to include wireless charging infrastructures. In the next years, addressing these critical features, is an essential way to improve the technology of wireless charging and then enhance vehicle electrification and sustainability of electro-mobility.

Acknowledgements

The author wishes to acknowledge with gratitude current and past PhD students for their essential contributions: Vincenzo Cirimele, Ping-Ping Ding, Shuoliang Ding, Mohammad Ibrahim, Paul Lagouanelle, Yao Pei.

Disclosure statement

No potential conflict of interest was reported by the author(s).

Notes on contributor

Lionel Pichon received the Dip. Eng. from Ecole Supérieure d'Ingénieurs en Electronique et Electrotechnique in 1984. In 1985 he joined the Laboratoire de Génie Electrique de Paris where he earned a PhD in electrical engineering in 1989. He got a position at the CNRS (Centre National de la Recherche Scientifique) in 1989. He is now Directeur de Recherche (Senior Research Scientist) in GeePs (Group of electrical engineering – Paris), a laboratory belonging to four institutions: CNRS, CentraleSupélec, Université Paris-Saclay, Sorbonne Université. His research interests include computational electromagnetics for wave propagation, scattering and electromagnetic compatibility. He is author or co-author of more than 120 journal papers.

References

[1] Rim CT, Mi C. Wireless power transfer for electric vehicles and mobile devices. New York: John Wiley & Sons, Ltd; 2017.
[2] Valtchev S, Borges B, Brandisky K, et al. Resonant contactless energy transfer with improved efficiency. IEEE Trans Power Electron. 2009;24(3):685–699.
[3] Wang CS, Stielau OH, Covic GA. Design consideration for a contactless electric vehicle battery charger. IEEE Trans Ind Electron. 2005;52(5):1308–1313.
[4] Sallán J, Villa JL, Llombart A, et al. Optimal design of ICPT systems applied to electric vehicle battery charge. IEEE Trans Ind Electron. 2009;56(6):2140–2149.
[5] Wang CS, Covic GA, Stielau OH. Power transfer capability and bifurcation phenomena of loosely coupled inductive power transfer system. IEEE Trans Ind Electron. 2004;51(1):148–157.
[6] Cirimele V. Design and integration of a dynamic IPT system for automotive applications. PhD dissertation, Politecnico di Torino and University Paris-Saclay; 2017.
[7] Cirimele V, Diana M, Freschi F, et al. Inductive power transfer for automotive applications: state-of-the-art and future trends. IEEE Trans Ind Appl. 2018;54(5):4069–4079.
[8] Ahmad A, Saad Alam M, Chabaan R. A comprehensive review of wireless charging technologies for electric vehicles. IEEE Trans Transport Elect. 2018;4(1):38–63.
[9] Fuad Abdul Aziz A, Fakhizan Romlie M, Baharudin Z. Review of inductively coupled power transfer for electric vehicle charging. IET Power Electron. 2019;12(14):3611–3623.
[10] Brown WC. The history of power transmission by radio waves. IEEE Trans Microw Theory Tech. 1984;32(9):1230–1242.
[11] Tesla N. Apparatus for transmission of electrical energy, May 15 1900. US Patent 649,621.
[12] George Iljitch Babat, High frequency electric transport system with contactless transmission of energy, September 1951. Application number GB926946A.
[13] Otto DV. Power supply equipment for electrically-driven vehicle, June 19 1974. JP Patent 49 063 111.
[14] Shladover SE, et al. Path at 20-history and major milestones. IEEE Trans Intell Transp Syst. 2007;8(4):584–592.
[15] Boys J, Green A. Inductive power pick-up coils, WO Patent App. PCT/NZ1994/000,115, Apr. 27, 1995. [Online]. Available from: https://www.google.com/patents/WO1995011545A1?cl = en.
[16] Boys JT, Green AW. Flux concentrator for an inductive power transfer system, US Patent 5,821,638, Oct. 13, 1998. [Online]. Available from: https://www.google.com/patents/US5821638.
[17] WAVE website. [cited 2020 Jan]. Available from: https://www.waveipt.com/.
[18] [Cited 2020 Jan]. Available from: https://www.bombardier.com/fr/media/newsList/details.bt_20150901_-berlin-erste-hauptstadt-mit-kabellos-geladener-e-bu.bombardiercom.html.
[19] Suh I. Application of shaped magnetic field in resonance (SMFIR) technology to future urban transportation, in CIRP design conference, 2011.

[20] Ahn S, Kim J. Magnetic field design for high efficient and low EMF wireless power transfer in on-line electric vehicle. Antennas and Propagation (EUCAP), Proceedings of the 5th European conference; 2011, p. 3979–3982.
[21] Huh J, Lee SW, Lee WY, et al. Narrow-width inductive power transfer system for online electrical vehicles. Power Electron IEEE Trans. 2011;26(12):3666–3679.
[22] Carlson RW, Normann B. Test results of the plugless inductive charging system from evatran group, Inc. SAE Int J Alt Powertrains. 2014;3:64–71.
[23] Budhia M, Covic GA, Boys JT. Design and optimization of circular magnetic structures for lumped inductive power transfer systems. IEEE Trans Power Electron. 2011;26(11):3096–3108.
[24] Budhia M, Boys JT, Covic GA, et al. Development of a single-sided flux magnetic coupler for electric vehicle IPT charging systems. IEEE Trans Ind Electron. 2013;60(1):318–328.
[25] Valtchev S, Borges B, Brandisky K, et al. Resonant contactless energy transfer with improved efficiency. IEEE Trans on Power Electron. 2009;24(3):685–699.
[26] Mohammad M, Tezera Wodajo E, Choi S, et al. Modeling and design of passive shield to limit EMF emission and to minimize shield loss in unipolar wireless charging system for EV. IEEE Trans Power Electron. 2019;34(12):12235–12245.
[27] ICNIRP. Guidelines for limiting exposure to time-varying electric, magnetic and electromagnetic fields (up to 300 GHz). Health Phys. 1998;74:494–522.
[28] ICNIRP. ICNIRP statement V guidelines for limiting exposure to time-varying electric and magnetic fields (1 Hz to 100 kHz). Health Phys. 2010;99:818–836.
[29] IEEE standard for safety levels with respect to human exposure to radio frequency electromagnetic fields, 3 kHz to 300 GHz. International committee on electromagnetic safety, the institute of electrical and electronics engineers, Inc. 3 Park Avenue, IEEE C95.1, IEEE Standards Dept., New York (NY); 2005.
[30] Kumar Kushwaha B, Rituraj G, Kumar P. 3-D analytical model for computation of mutual inductance for different misalignments With shielding in wireless power transfer system. IEEE Trans Transport Elect. 2017;3(2):332–342.
[31] Dashora HK, Buja G, Bertoluzzo M, et al. Analysis and design of DD coupler for dynamic wireless charging of electric vehicles. J Electromagn Wave Appl. 2018;32(22):170–189.
[32] Wang S, Dorrell DG. Loss analysis of circular wireless EV charging coupler. IEEE Trans Magn. 2014;50(11). article 8402104.
[33] Marques EG, Mendes AMS. Comparison of magnetic coupling structures for IPT systems. COMPEL – Int J Comput Math Electr Electron Eng. 2015;34(2):514–530.
[34] Kim M, Byun J, Lee BK. Performance analysis of magnetic power pads for inductive power transfer systems with ferrite structure variation. J Electr Eng Technol. 2017;12(3):1211–1218.
[35] Kim M, Joo D-M, Lee BK. Design and control of inductive power transfer system for electric vehicles considering wide variation of output voltage and coupling Coefficient. IEEE Trans Power Electron. 2019;34(2):1197–1218.
[36] Wei XC, Li EP. Simulation and experimental comparison of different coupling mechanisms for the wireless electricity transfer. J Electromagn Waves Appl. 2009;23:925–934.
[37] Shia X, Qia C, Qua M, et al. Effects of coil shapes on wireless power transfer via magnetic resonance coupling. J Electromagn Wave Appl. 2014;28(11):1316–1324.
[38] Naik Mudea K, Bertoluzzoa M, Bujaa G, et al. Design and experimentation of two-coil coupling for electric city-car WPT charging. J Electromagn Wave Appl. 2016;30(1):70–88.
[39] Ibrahim M, Bernard L, Pichon L, et al. Electromagnetic model of EV wireless charging systems in view of energy transfer and radiated field control. Int J Appl Electromagn Mech. 2014;46(2):355–360.
[40] Ibrahim M, Pichon L, Bernard L, et al. Advanced modeling of a 2-kW series-series resonating inductive charger for real electric vehicle. IEEE Trans Vehi Technol. Feb 2015;64:421–430.
[41] Zaheer A, Hao H, Covic GA, et al. Investigation of multiple decoupled coil primary pad topologies in lumped IPT systems for interoperable electric vehicle charging. IEEE Trans Power Electron. 2015;30(4):1937–1955.

[42] Zhang W, White JC, Abraham AM, et al. Loosely coupled Transformer structure and interoperability study for EV wireless charging systems. IEEE Trans Power Electron. 2015;30(11):6356–6367.
[43] Ahmad A, Alam MS, Mohamed AAS. Design and interoperability analysis of Quadruple Pad structure for electric vehicle wireless charging application. IEEE Trans Transport Elect. 2019;5(4):934–945.
[44] Ibrahim M, Bernard L, Pichon L, et al. Inductive charger for electric vehicle: advanced modeling and interoperability analysis. IEEE Trans Power Elect. 2016;31(12):8094–8114.
[45] Nadakuduti J, Douglas M, Lu L, et al. Compliance demonstration of wireless power charging systems with respect to human safety limits. IEEE Trans Electromagn Compat. 2015;30(11):6264–6273. DOI:10.1109/TPEL.2015.2400455.
[46] Laakso I, Tsuchida S, Hirata A, et al. Evaluation of SAR in a human body model due to wireless power transmission in the 10 MHz band. Phys Med Biol. 2012;57(15):4991–5002.
[47] Christ A, Douglas MG, Roman J, et al. Evaluation of wireless resonant power transfer systems with human electromagnetic exposure limits. IEEE Trans Electromagn Compat. 2013;55(2):265–274.
[48] Gabriel C, Gabriel S, Corthout E. The dielectric properties of biological tissues: I. literature survey. Phys Med Biol. 1996;41:2231–2249.
[49] Durney CH, Iskander MF, Massoudi H, et al. An empirical formula for broad-band SAR calculations of prolate spheroidal models of humans and animals. IEEE Trans Microw Theory Tech. 1979;27(8):758–763.
[50] Christ A, Kainz W, Hahn EG, et al. The Virtual FamilyVDevelopment of surface based anatomical models of two adults and two children for dosimetric simulations. Phys Med Biol. 2010;55(2):23–38.
[51] Caon M. Voxel-based computational models of real human anatomy: a review. Radiation Environ Biophys. 2004;42(4):229–235.
[52] Nagaoka T, Watanabe S, Sakurai K, et al. Development of realistic high-resolution whole-body voxel models of Japanese adult males and females of average height and weight, and application of models to radio-frequency electromagnetic-field dosimetry. Phys Med Biol. 2004;49(1):1–15.
[53] Zaidi H, Xu XG. Computational anthropomorphic models of the human anatomy: the path to realistic Monte Carlo modeling in radiological sciences. Annu Rev Biomed Eng. 2007;9:471–500.
[54] Zaidi H, Tsui B. Review of computational anthropomorphic anatomical and physiological models. Proc IEEE. 2009;97(12):1938–1953.
[55] IT'IS Foundation, the virtual population, Zurich, Switzerland; 2012. [Online]. Available from: https://www.itis.ethz.ch/services/ anatomical-models/overview/.
[56] Cherubini E, Chavannes N, Kuster N. Anatomical-based deformation of 3-D CAD high-resolution human models for complex electromagnetic simulations. Presented at the Joint Meeting Bioelectromagnetics Society/Europe Bioelectromagnetics Association, Davos (Switzerland); June 2009.
[57] Cvetkovic M, Poljak D. Electromagnetic-thermal dosimetry comparison of the homogeneous adult and child brain models based on the SIE approach. J Electromagn Wave Appl. 2015;29(17):2365–2379.
[58] Wu T, Tan L, Shao Q, et al. Chinese adult anatomical models and the application in evaluation of wideband RF EMF exposure. Phys Med Biol. 2011;56:2075–2089.
[59] Dahdouh S, Varsier N, Serrurier A, et al. A comprehensive tool for image-based generation of fetus and pregnant women mesh models for numerical dosimetry studies. Phys Med Biol. 2014;59(16):4583–4602.
[60] Yee KS. Numerical solution of initial boundary value problems involving Maxwell's equations in isotropic media. IEEE Trans Antennas Propag. 1966;14(3):585–589.
[61] Hadjem A, Lautru D, Dale C, et al. Study of specific absorption rate (SAR) induced in two child head models and in adult heads using mobile phones. IEEE Trans Microw Theory Tech. 2005;53(1):4–11.

[62] Chiaramello E, Parazzini M, Fiocchi S, et al. Stochastic dosimetry based on low rank tensor approximations for the assessment of children exposure to WLAN source. IEEE J Electromagn RF Microwave Med Biol. 2018;2(2):131.
[63] Cimala C, Clemens M, Streckert J, et al. Simulation of inductive power transfer systems exposing a human body with a coupled scaled-frequency approach. IEEE Trans Magn. 2017;53(6), paper 7201804.
[64] Bakker J, Paulides M, Neufeld E, et al. Children and adults exposed to low-frequency magnetic fields at the ICNIRP reference levels: theoretical assessment of the induced electric fields. Phys Med Biol. 2012;57(7):1815–1829.
[65] Christ A, Guldimann R, Bühlmann B, et al. Exposure of the human body to professional and domestic induction cooktops compared to the basic restrictions. Bioelectromagnetics. 2012;8:695–705.
[66] Chen XL, Umenei AE, Baarman DW, et al. Human exposure to close-range resonant wireless power transfer systems as a function of design parameters. IEEE Transa Electromagn Compat. 2014;56(5):1027–1034.
[67] Iwamoto T, Arima T, Uno T, et al. Measurement of electromagnetic field in the vicinity of wireless power transfer system for evaluation of human-body exposure, EMC, Tokyo; 2014.
[68] Yavolovskaya E, Chiqovani G, Gabriadze G, et al. Simulation of human exposure to electromagnetic fields of inductive wireless power transfer systems in the frequency range from 1 Hz to 30 MHz. Proceeding of the 2016 international symposium on electromagnetic compatibility – EMC EUROPE 2016, Wroclaw (Poland), September 5–9, 2016.
[69] Chakarothai J, Wake K, Arima T, et al. Exposure evaluation of an actual wireless power transfer system for an electric vehicle with near-field measurement. IEEE Trans Microw Theory Tech. 2018;66(3):1543–1552.
[70] Park S. Evaluation of electromagnetic exposure during 85 kHz wireless power transfer for electric vehicles. IEEE Trans Magnet. 2018;53(1). paper 5100208.
[71] Wang Q, Li W, Kang J, et al. Electromagnetic safety evaluation and protection methods for a wireless charging system in an electric vehicle. IEEE Trans Electromagn Compat. 2019;61(6):1913–1925.
[72] Li JC, Huang X, Chen C, et al. Effect of metal shielding on a wireless power transfer system. AIP Adv. 2017;7(5). Art. no. 056675.
[73] Kim J, et al. Coil design and shielding methods for a magnetic resonant wireless power transfer system. Proc IEEE. 2013;101(6):1332–1342.
[74] Kim H, Cho J, Ahn S, et al. Suppression of leakage magnetic field from a wireless power transfer system using ferromagnetic material and metallic shielding. Proceeding IEEE international symposium on electromagnetic compatibility, Pittsburgh (PA); Aug. 2012, p. 640–645.
[75] Hiles ML, Olsen RG, Holte KC, et al. Power frequency magnetic field management using a combination of active and passive shielding technology. IEEE Trans Power Del. 1998;13(1):171–179.
[76] Kim SM, Moon JI, Cho IK, et al. Advanced power control scheme in wireless power transmission for human protection from EM field. IEEE Trans Microw Theory Techn. 2015;63(3):847–856.
[77] Campi T, Cruciani S, Maradei F, et al. Near field reduction in a wireless power transfer system using LCC compensation. IEEE Trans Electromag Compat. 2017;59(2):686–694.
[78] Campi T, Cruciani S, Feliziani M. Numerical characterization of the magnetic field in electric vehicles equipped with a WPT system. Wireless Power Transfer. 2017;4:78–87.
[79] Campi T, Cruciani S, Feliziani M. Wireless power transfer (WPT) system for an electric vehicle (EV): How to shield the car from the magnetic field generated by two planar coils. Wireless Power Transfer. 2017;5:1–8.
[80] Lee S, Kim D-H, Cho Y, et al. Low leakage electromagnetic field level and high efficiency using a novel hybrid loop-array design for wireless high power transfer system. IEEE Trans Ind Electron. 2019;66(6):4356–4367.
[81] Ding P, Pichon L, Bernard L, et al. Electromagnetic fields in human body by wireless inductive system. COMPEL: Int J Comput Math Elect Electron Eng. 2015;34(2):590–595.
[82] Jokela K. Restricting exposure to pulsed and broadband magnetic fields. Health Phys. 2000;79(4):373–388.

[83] Cirimele V, Fabio F, Luca G, et al. Human exposure assessment in dynamic inductive power transfer for automotive applications. IEEE Transactions on Magnetics. Inst Elect Electron Eng. 2017;53(6):5000304.
[84] Kroese D, Taimre T, Botev Z. Handbook of Monte Carlo methods. New York: Wiley Series in Probability and Statistics; 2011.
[85] Koziel S, Bekasiewicz A. Low-cost surrogate-assisted statistical analysis of miniaturized microstrip couplers. J Electromagn Wave Appl. 2016;30(10):1345–1353.
[86] Lefebvre J, Roussel H, Walter E, et al. Prediction from wrong models: the Kriging approach. IEEE Antennas Propag Mag. 1996;38(4):35–45.
[87] Voyer D, Musy F, Nicolas L, et al. Probabilistic methods applied to 2D electromagnetic numerical dosimetry. COMPEL. 2008;27(3):651–667.
[88] Silly-Carette J, Lautru D, Wong M-F, et al. Variability on the propagation of a plane wave using stochastic collocation methods in a bio electromagnetic application. IEEE Microwave Wireless Comp Lett. 2009;19(4):185–187.
[89] Kersaudy P, Sudret B, Varsier N, et al. A new surrogate modeling technique combining Kriging and polynomial chaos expansions–application to uncertainty analysis in computational dosimetry. J Comput Phys. 2015;286:103–117.
[90] Liorni I, Parazzini M, Fiocchi S, et al. Study of the influence of the orientation of a 50-Hz magnetic field on fetal exposure using polynomial chaos decomposition. Int J Environ Res Public Health. 2015;12:5934–5953.
[91] Bilicz S, Gyimóthy S, Pávó J, et al. 2016. Uncertainty quantification of wireless power transfer systems. 2016 IEEE Wireless Power Transfer Conference (WPTC), Aveiro, 2016, pp. 1–3. DOI:10.1109/WPT.2016.7498861.
[92] Knaisch K, Gratzfeld P. Gaussian process surrogate model for the design of circular, planar coils used in inductive power transfer for electric vehicles. IET Power Electron. 2016;9(15):2786–2794.
[93] Lagouanelle P, Krauth V-L, Pichon L. uncertainty quantification in the assessment of human exposure near wireless power transfer systems in automotive applications, automotive, Turin (Italy); 2019.
[94] Sudret B. Global sensitivity analysis using polynomial chaos expansions. Reliab Eng Syst Safe. 2008;93(7):964–979.
[95] Blatman G, Sudret B. Adaptive sparse polynomial chaos expansion based on least angle regression. J Comput Phys. 2011;230(6):2345–2367.
[96] Sobol IM. Sensitivity estimates for nonlinear mathematical models. Mathe Model Comput Exper. 1993;1(4):407–414.
[97] Larbi M, Stievano IS, Canavero FG, et al. Variability impact of many design parameters: the case of a realistic electronic link. IEEE Trans Electromagn Compat. 2018;60(1):34–41.
[98] Lagouanelle P, Krauth V-L, Pichon L. Uncertainty quantification in the assessment of human exposure near wireless power transfer systems in automotive applications, automotive, Turin (Italy); 2019.
[99] Gori P-A, Sadarnac D, Caillierez A, et al. Sensorless inductive power transfer system for electric vehicles: strategy and control for automatic dynamic operation, 2017 19th European conference on power electronics and applications (EPE'17 ECCE Europe), Warsaw (Poland).
[100] Zucca M, Bottauscio O, Harmon S, et al. Metrology for inductive charging of electric vehicles (MICEV). Proceeding international conference of electrical and electronic technologies for automotive, Turin (Italy), July 2019.
[101] MICEV, MICEV project homepage. [Online]. [cited Jan 2020]. Available from: https://www.micev.eu/.
[102] S. Marelli, and B. Sudret, UQLab: a framework for uncertainty quantification in Matlab. Proceeding 2nd international conference on vulnerability, risk analysis and management (ICVRAM2014), Liverpool (UK); 2014, p. 2554–2563.
[103] Lagouanelle P, Bottauscio O, Pichon L, et al. Impact of parameters variability on the level of human exposure due to inductive power transfer. IEEE CEFC 2020 (Biennal of Electromagnetic Field Computation), Pisa (Italy), November 2020.

[104] Mohamed AAS, An S, Mohammed O. Coil design optimization of power pad in IPT system for electric vehicle applications. IEEE Trans Magn. 2018;54(4). Article no. 9300405.
[105] Otomo Y, Igarashi H. A 3-D topology optimization of magnetic cores for wireless power transfer device. IEEE Trans Magn. 2019;55(6). Article no. 8103005.
[106] Lu M, Ngo KDT. A fast method to optimize efficiency and stray magnetic field for inductive-power-transfer coils using lumped-loops model. IEEE Transa Power Electronic. 2019;33(4):3065–3075.
[107] Cruciani S, Campi T, Maradei F, et al. Active shielding design for wireless power transfer systems. IEEE Trans Electromagn Compat. 2019;61(6):1953–1960.
[108] Fabric EU project final event & demonstration video. [Online]. [cited Jan 2020]. Available from: https://www.youtube.com/watch?v = ngrJ60o06f8.